A Four-gene Autophagy-related Prognostic Signature and Its Association With Immune Landscape in Lung Squamous Cell Carcinoma

Lumeng Luo
Fudan University Shanghai Cancer Center Department of Radiation Oncology: Fudan University Shanghai Cancer Center Radiation Oncology Research Center

Minghe Lv
Fudan University Shanghai Cancer Center Department of Radiation Oncology: Fudan University Shanghai Cancer Center Radiation Oncology Research Center

Xuan Li
Jinshan hospital Fudan University

Tiankui Qiao
Jinshan hospital Fudan University

Kuaile Zhao
Fudan University Shanghai Cancer Center Department of Radiation Oncology: Fudan University Shanghai Cancer Center Radiation Oncology Research Center

Jiaying Deng (17111230042@fudan.edu.cn)
Fudan University Shanghai Cancer Center Department of Radiation Oncology: Fudan University Shanghai Cancer Center Radiation Oncology Research Center https://orcid.org/0000-0002-1744-1203

Primary research

Keywords: Lung Squamous Cell Carcinoma, Autophagy, Prognostic Signature, Immune Landscape, Immune Infiltration, Bioinformatic Analysis

Posted Date: December 14th, 2020

DOI: https://doi.org/10.21203/rs.3.rs-125355/v1

Abstract

Background: Recent advances in immune checkpoint inhibitors (ICIs) have dramatically changed the therapeutic strategy against lung squamous cell carcinoma (LUSC). In the era of immunotherapy, effective biomarkers to better predict outcomes and inform treatment decisions for patients diagnosed with LUSC are urgently needed. We hypothesized that immune contexture of LUSC is potentially dictated by tumor intrinsic events, such as autophagy. Thus, we attempted to construct an autophagy-related risk signature and examine its prediction value for immune phenotype in LUSC.

Method: The expression profile of LUSC was obtained from the cancer genome atlas (TCGA) database and the profile of autophagy-related genes (ARGs) was extracted. The survival-related ARGs (sARGs) was screened out through survival analyses. Random forest was performed to select the sARGs and construct a prognostic risk signature based on these sARGs. The signature was further validated by receiver operating characteristic (ROC) analysis and Cox regression. GEO dataset was used as an independent testing dataset. Patients were divided into high-risk and low-risk group based on the risk score. Then, gene set enrichment analysis (GSEA) was conducted between the two groups. The Single-Sample GSEA (ssGSEA) was introduced to quantify the relative infiltration of immune cells. The correlations between risk score and several main immune checkpoints were examined. And the ESTIMATE algorithm was used to calculate the estimate/immune/stromal scores of the LUSC.

Results: Four ARGs (CFLAR, RGS19, PINK1 and CTSD) with the most significant prognostic values were enrolled to construct the risk signature. Patients in high-risk group had better prognosis than the low-risk group ($P < 0.0001$ in TCGA; $P < 0.01$ in GEO) and considered as an independent prognosis factor. We also found that high-risk group indicated an immune-suppression status and had higher levels of infiltrating regulatory T cells and macrophages, which are correlated with worse outcome. Besides, risk score showed a significantly positive correlation with the expression of PD-1 and CTLA4, as well as estimate score and immune score.

Conclusion: This study established a novel autophagy-related four-gene prognostic risk signature, and the autophagy-related scores are associated with immune landscape of LUSC, with higher score indicating a stronger immune-suppression status.

Background

Lung cancer is the second most common cancer, and is the leading cause of cancer death worldwide [1]. Lung squamous cell carcinoma (LUSC), a subtype of non-small cell lung cancer (NSCLC), comprises one of the main histological types of lung cancer [2]. Unlike lung adenocarcinoma, no first-line targeted therapies are clinically available in LUSC patients [3]. In recent years, immune checkpoint inhibitors(ICIs) targeting the programmed death ligand-1 (PD-L1)/PD-1 immune checkpoint axis has shown some promising results in the treatment of NSCLC, including LUSC [4]. However, it seems that only a fraction of patients benefit from immunotherapy, probably due to the tumor intrinsic heterogeneity and variation in

tumor immune microenvironment [4]. More effective biomarkers for prognosis and optimal treatment selection are urgently needed. Therefore, it is vital to find more effective and precise methods for outcome predicting in LUSC.

Autophagy, an intracellular lysosomal degradation pathway that supports nutrient recycling and metabolic adaptation, is supposed to protect cells and tissues from stressors in normal physiological processes [5]. A growing evidence suggested that autophagy also plays an important role in various pathological processes, especially in cancer [5]. In the earliest stages of tumorigenesis, autophagy may limit the development of tumors [6]; however, during the advanced stages of tumors, autophagy is upregulated, and promotes tumor cell proliferation through absorb nutrients and energy driving from degraded proteins and organelles [7]. Autophagy can help cope with intracellular and environmental stresses, such as hypoxia, nutrient shortage, or cancer therapy, thereby favoring tumor progression [5, 8, 9]. In the tumor microenvironment, autophagy is an important regulator of immune responses, modulating the functions of immune cells and the production of cytokines [10]. Autophagy seems to be a “double-edged sword” in immune cells within the tumor microenvironment. It can promote or suppress tumor development, which depends on the properties of the tumor and cell types.

With the great success of PD-L1 /PD-1 inhibitors and other ICIs in NSCLC, there arise the question of how autophagy would affect cancer treatments in the age of immunotherapy. A comprehensive understanding of autophagy-related genes (ARGs) associated the immune microenvironment would favor the expansion of immunotherapies and explore the predictive biomarkers for the design of patient-tailored combination treatments. At present, few studies have systematically explored the correlation between autophagy and immune microenvironment of LUSC. Moreover, whether ARGs and immune infiltration level could be prognostic in LUSC subtype remains to be fully elucidated.

Therefore, in this study, using the transcriptomic data of LUSC from the TCGA dataset, we developed a prognostic risk signature based on four ARGs in LUSC by random forest algorithm and then explore whether it correlates with the immune landscape. The results shine light on clarifying the association of ARGs and immune escape, and establish a more personalized precision predicting model for immunotherapy.

Methods

2.1 Data Collection

We collected all transcriptome profiles of LUSC available in the database of TCGA (https://portal.gdc.cancer.gov/).Corresponding clinical information of these patients including gender, age, pathological stage, TNM stage, follow-up time, survival status was also obtained from TCGA (Samples missing any clinical characteristics were excluded and samples of which OS ≤ 30 days were also excluded because these patients probably died of unpredictable factors). Our study included the expression profile of 32 normal samples and 326 LUSC samples. As the status of distant metastasis is

missing in lots of samples, we didn't take the status of M stage into consideration in the current study. From the GEO dataset (https://www.ncbi.nlm.nih.gov/geo/), transcriptome data of GSE41271 were obtained. A total of 78 LUSC subtype samples from GSE41271 with available clinical and survival data was utilized as an independent validation cohort.

2.2 Acquisition of ARGs

The Human Autophagy Database (HADb, http://www.autophagy.lu/) provides a complete and real-time updated list of human genes related with the biological processes of autophagy reported in PubMed or other common databases [11]. We got 232 ARGs form HADb, among which 224 genes were available in the expression profile from TCGA (The gene list is showed in Table S1).

2.3 Differentially Expressed Analysis of ARGs and Functional Enrichment Analysis

To compare the expression level of ARGs between tumor and normal sample, differentially expressed analysis on all ARGs was conducted based on Wilcoxon-test with edgeR package under R environment (version 3.6.3). The cut-off criterion for differentially expressed genes (DEGs) was set as $p < 0.05$ and $\log2 |\text{fold change}| > 1$. The results are displayed with pheatmap package. Then, We performed Kyoto Encyclopedia of Genes and Genomes (KEGG) pathway enrichment analysis to explore the main roles of disordered differentially expressed ARGs (DE-ARGs) in LUSC. The cut-off criterion was $p < 0.05$ and Benjamin-Hochberg adjusted $p < 0.05$. The analyses and the visualization of results were conducted under R environment with ClusterProfiler package.

2.4 Survival-related ARGs (sARGs)

The ARGs associated with clinical outcomes in LUSC patients were identified as sARGs. sARGs were selected by Kaplan–Meier method and verified using a log-rank test conducted by the R packages survival and survminer (The cut-off value of the expression level of each gene was 50%, $P < 0.05$). Final 54 survival-related ARGs were found. These sARGs were specified for subsequent research.

2.5 Construction and validation of Autophagy-Related Prognostic Signature

We used random survival forest (RSF) method for developing a prognosis model based on sARGs. The random forest algorithm is a machine learning strategy, which is based on the construction of many classification (decision) trees that are used to classify the input data vector [12]. Using "RandomForestSRC" package for R, four genes were considered important survival relevant variables for subsequent analysis. The developed RSF prognosis model based on the optimal parameters was then evaluated on the independent dataset where the RSF-based score was derived for each sample. Then, to verify the validity and robustness of the RSF prognosis model, standard Kaplan–Meier survival curves were generated for different risk patient groups on the basis of the RSF-based scores. Based on the optimal cutoff values obtained by the "survminer" R package, LUSC patients were classified as low-risk

and high-risk according to their risk score. To appraise the prognostic performance of the model, Kaplan-Meier analysis and the log-rank test were employed. Time-dependent receiver operating characteristic (ROC) curves were depicted to evaluate the sensitivity and specificity using the “timeROC” R package [13]. Area under the curve (AUC) values were calculated from the ROC curves. We then performed univariate and multivariate Cox regression analyses to verify the prognostic value of the risk score. We took age, gender, TNM stage (M stage excluded) as candidate risk factors for regression analyses. We evaluated if all these factors are risk factors for poor prognosis by univariate Cox regression analysis, and then by multivariate Cox regression, further determined if the risk score could be utilized for predicting the prognosis of LUSC patients independently.

2.6 Gene Set Enrichment Analysis (GSEA)

GSEA was conducted to explore significant immune phenotypes between the two groups (high- and low-risk groups) [14]. The gene sets involved in the negative-regulation of immune response was imported from MSIGDB gmt file from Broad institute. We performed GSEA using “Clusterprofiler” R package and “GSEABase” R package. The cutoff criterion for statistically significant terms was set as $p < 0.05$.

2.7 Immune Cell Infiltration

The Single-Sample Gene Set Enrichment Analysis (ssGSEA) was introduced to quantify the relative infiltration of 28 immune cell types in the tumor microenvironment. “GSVA” R package was used in the analysis. Feature gene panels for each immune cell type were obtained from previous studies [15, 16]. The relative abundance of each immune cell type was represented by an enrichment score from ssGSEA analysis.

2.8 ESTIMATE Algorithm

The ESTIMATE((Estimation of Stromal and Immune cells in Malignant Tumor tissues using Expression data)) algorithm was applied to the normalized expression matrix for estimating the stromal and immune scores using "estimate" package (http://r-forge.r-project.org; repos = rforge, dependencies = TRUE) for each LUSC sample [17].

2.9 Statistical Analysis

Statistical analyses of this study were conducted using the R software (version 3.6.3), and $P < 0.05$ was regarded as significant.

Results

3.1 Identification of Differentially Expressed Autophagy-Related Genes(ARGs)

Based on the edgeR algorithm and according to the screening criteria of DEGs, 48 of the 224 ARGs (Table S1) showed significant alterations of expression levels in LUSC compared with normal control, including

20 up-regulated and 28 down-regulated genes, respectively ($p < 0.05$ and log2 |fold change| > 1). The results are shown in a heatmap (Figure 1A). These differentially expressed ARGs (DE-ARGs) were then selected for KEGG pathway enrichment analysis with a threshold of $p < 0.05$. As shown in Figures 1B, the differentially expressed ARGs were mainly enriched in regulation of autophagy, apoptosis and mitophagy. It is also worth noting that “PD-L1 expression and PD-1 checkpoint pathway in cancer” were enriched, implicating the correlation between these ARGs and immunosuppression pathway.

3.2 Construction of the Autophagy-related Prognostic Signature

The Kaplan–Meier method and log-rank test were applied to examine the relationship between overall survival (OS) and all ARGs (rather than DE-ARGs) in 326 LUSC samples from TCGA. As shown in Table S2, 54 genes were significantly related with OS of LUSC patients ($p < 0.05$) and these genes were defined as survival-related ARGs (sARGs). Meanwhile, we noticed that not all sARGs are DE-ARGs. Next, Random Forest was performed to select sARGs with the best prognostic value and to build an autophagy-related risk score model in the TCGA cohort. Four sARGs including CFLAR, RGS19, PINK1 and CTSD were selected as most important survival relevant variables. The Kaplan-Meier overall survival (OS) curves of these four genes were displayed in Figure 2 (The cutoff value of gene expression level was 50%). The random survival forest -based score was derived for each sample and defined as risk score. Patients in the TCGA cohort (training dataset) then were assigned to a high-risk or low-risk group using the optimal cut-off value obtained with the “survminer” R package. Risk score distribution and corresponding four -gene expression patterns were shown in Figure 3A. With the increase of risk score, the expression levels of the four genes were elevated. The overall survival time of the high-risk group was shorter than that of the low-risk group.

3.3 Validation of the Autophagy-related Prognostic Signature

For further validation, 78 samples of LUSC subtype from GSE41271 (GEO dataset) were derived as an independent testing dataset. Then, Kaplan-Meier analysis were applied to the two cohorts and demonstrated that patients with a high-risk score were correlated with worse outcomes in the two cohorts (Figure 3B-C). Besides, the time-dependent ROC curve analysis of the risk score model in the TCGA cohort indicated a promising prognostic ability for OS (1-year AUC = 0.948, 3-year AUC = 0.965, 5-year AUC = 0.97, Figure 3D). Meanwhile, the ROC curve of OS prediction was drawn in GEO cohort (1-year AUC = 0.649, 3-year AUC = 0.559, 5-year AUC = 0.655, Figure 3E). The autophagy-related model showed a less promising prognostic ability in GEO cohort than the TCGA cohort, possibly due to the small sample size of GEO dataset (78 in GEO vs. 326 in TCGA), which deserved further large samples to validate. Furthermore, in TCGA cohort, we took age, gender, TNM stage (M stage excluded) as candidate risk factors for Cox regression analyses. As shown in Table 1, univariate Cox regression analysis indicated

that N stage and risk score are risk factors for poor prognosis, and multivariate Cox regression demonstrated the independence of risk score of this signature in prognosis prediction from other clinical factors.

3.4 High Risk Group Indicated an Immune-suppression status

To explore the immune phenotype and the potential immune-related mechanisms underlying our constructed prognostic gene signature, GSEA was performed to find enriched immune-related gene sets annotated by the gene ontology (GO) term. Results unveiled that seven significantly altered immune-related pathways were enriched in high-risk group, and no immune-related pathways were enriched in the low-risk group (Figure 4). High risk score was significantly associated with the macrophage activation involved in immune response ($P < 0.05$), negative regulation of adaptive immune response ($P < 0.01$), negative regulation of immune effector process ($P < 0.01$), negative regulation of immune system process ($P < 0.01$), negative regulation of innate immune response ($P < 0.01$), negative regulation of adaptive immune response ($P < 0.01$), and negative response of immune response ($P < 0.01$). Consistently, high-risk group exhibited an immunosuppressive phenotype.

3.5 High Risk Group showed an increased Infiltration of suppressive immune cell populations

To further investigate whether there is an association between autophagy-related score and the regulation of suppressive immune cell populations, normalized ssGSEA scores of 28 infiltrating immune cell populations in each sample were calculated and represented their infiltration level. We drew a heatmap to visualize the relative abundance of 28 infiltrating immune cell populations (Figure 5). And the boxplot of these immune cells labeled with the P value of Wilcoxon rank test between low-risk and high- risk score group was shown in Supplementary Figure 1. We observed a positive correlation between risk score and the infiltration levels of most immune cell subtypes, including cell types executing anti-tumor immunity (Activated CD4 T cell, Activated CD8 T cell, Central memory CD4 T cell, Central memory CD8 T cell, Effector memory CD4 T cell, Effector memory CD8 T cell, Type 1 T helper cell, Type 17 T helper cell, CD56bright natural killer cell) and cell types executing pro-tumor and immune suppressive functions (Regulatory T cell, Type 2 T helper cell, CD56dim natural killer cell, Immature dendritic cell, Macrophage, MDSC, Neutrophil, Plasmacytoid dendritic cell). For further investigation, Pearson's correlation analysis was applied to the abundances of these two categories of cells. Results showed that the abundances of anti-tumor immune cells were positively associated with the abundances of immunosuppression cells in tumor microenvironment (Figure 6A). And It seemed that immune suppression is stronger in high-risk group than low-risk group, which is consistent with GSEA results.

3.6 Macrophage and Regulatory T cell (Treg) correlated with worse outcome

Then, univariate Cox regression and Kaplan-Meier analysis plus the log-rank test were employed to select the prognostic immune cells among these 28 infiltrating immune cell subtypes. Results revealed that only macrophage and regulatory T cell have a significant correlation with overall survival. As shown in Figure 6D-E, higher infiltration of macrophage and regulatory T cell correlated with shorter overall survival time ($P < 0.05$). As above, high- risk group was associated with higher infiltration of macrophage and regulatory T cell ($P < 0.01$) (Figure 6B-C). This observation suggested macrophage and regulatory T cell may accounted for the poor prognosis induced by immunosuppression in high-risk group.

3.7 Correlation between genes expression and immunocyte infiltration

The correlations of the expression of four genes in this autophagy-related signature with the infiltration level of macrophage and regulatory T cell as well as risk score were investigated. Figure7A demonstrated overall correlations among these arguments. The four genes were strongly interrelated and exhibited significantly positive association with the infiltration of two immunocyte. Besides, the genes expression and immunocyte infiltration were increasing along with the growth of risk score.

3.8 Immune Checkpoints Analysis

Immune checkpoints inhibitors are becoming the promising strategies in the treatments of lung cancer. Therefore, we investigated the association of the risk score and the main immune checkpoints, including PD-1/PD-L1 and CTLA4. As Figure 7B-D shown, risk score showed a significantly positive correlation with PD-1 and CTLA4 ($P < 0.01$). While, there is no significant correlation between risk score and PD-L1 expression. In summary, high-risk group had higher levels of PD-1 and CTLA4. Then, we also examined the correlations between the expression of the four ARGs (CFLAR, RGS19, PINK1, CTSD) and the expression of immune checkpoints (PD-1, PD-L1, CTLA4). Results showed that the expressions of four ARGs had significant associations with the immune checkpoints consistently (only the correlation between PINK1 and PD-L1 was not significant) (Supplementary Figure 2).

3.9 Estimate score, immune score and stromal score

ESTIMATE (Estimation of Stromal and Immune cells in Malignant Tumor tissues using Expression data) is a newly developed algorithm that uses the transcriptional profiles of cancer tissues to infer the level of infiltrating stromal and immune cells based on specific gene expression signatures of stromal and immune cells in the specific cancer type. In the present study, the stromal score, immune score, and

estimate score of each included sample of was calculated by applying Estimate R package. Next, the association of autophagy-related risk scores with the estimate/immune/stromal scores was examined. As shown in Figure 8A-C, estimate score and immune score were found to have a positive correlation with the risk scores of our established model ($P < 0.05$). Stromal score was also rising with the increase of risk score, but not significantly ($P=0.072$). The prognostic value of the three types of score were also investigated. Survival analysis showed that the patients with higher estimate/immune/stromal score had a poorer overall survival, although the statistical significance were only observed in stromal score ($P < 0.05$).

Discussion

Over the past decade, new treatments for patients with LUSC have evolved dramatically, including immune checkpoint inhibitors and combination strategies. Thus, the more refined risk-stratification to guide treatment for LUSC patients beyond conventional TNM staging are needed. With the rapid development of high-throughput next generation sequencing, machine leaning, and bioinformatics analyses, prognostic signatures composed of a set of genes have been designed to meet this need. Compared to the single molecular predictors, signatures integrated the prognostic value of several genes and seemed to have a better outcome prediction ability. In previous studies, several risk signatures have shown satisfactory effects in outcome prediction and treatment guiding in lung cancer, such as miRNA-based signature [18], lncRNA-related signature [19], immune-associated signature [20]. These risk signatures could be used as the tailored algorithms to individualize therapy.

Autophagy, which induce degradation of proteins and organelles or cell death upon cellular stress, are crucial in the pathophysiology of malignant tumor [9, 21]. The apoptotic effect of autophagy is controversial as both inhibitory and stimulatory effects have been reported in NSCLC [21]. Consequently, an integrated study of multi-molecules genes model is needed to figure out the exact effects of autophagy in lung cancer. A previous study has reported an autophagy-associated multiple-gene signature that correlated with survival in NSCLC [22]. However, in the era of immunotherapy, the immune contexture of tumor microenvironment is essential for the treatment selection and survival prediction [23]. The correlations between autophagy and immune pathway should not be ignored [10]. Thus, in this study, we conducted a complete and meaningful analysis of autophagy-related genes involved in outcome prediction and associated immune landscape, which may also enable the identification of patients who are more likely to respond to immunotherapy. Moreover, different with previous studies, random forest instead of Lasso regression was applied in the current analyses. Random forest is a process of machine learning with accurate algorithms and high efficiency in classification prediction.

In the present study, four ARGs including CFLAR, RGS19, PINK1 and CTSD were screened out as most important survival relevant variables and were selected for the construction of an autophagy-related prognostic risk signature. CFLAR, also known as c-FLIPL, is a critical anti-apoptotic protein that inhibits cell death mediated by the death receptors Fas, DR4, DR5, and TNF-R1 [24, 25]. CFLAR was found as an independent adverse prognostic biomarker in different cancer types [26, 27]. Besides, elevated expression

of CFLAR is associated with tumor cells escaping from immune surveillance in vivo, correlates with a more aggressive tumor, and is also considered to be the main cause of immune escape [25]. A recent study reported that down regulation of CFLAR could enhance the antitumor response of T cells and enhances the PD-1 blockade efficacy in melanoma tumor model [28]. And knockdown of CFLAR could also decrease the expression of PD-L1 [28]. Consistent with these results, our analyses found that high expression of CFLAR was significantly associated with some key immune checkpoint including PD-1, PD-L1 and CTLA4 (Supplementary Fig. 2). These findings may provide a new combined therapeutic target for further improving the efficacy of ICIs. RGS19 is a member of the regulators of G protein signaling (RGS proteins) [29]. Rapid termination of G protein signals by RGS proteins can potentially modulate growth signals and hence promote tumorigenesis, although no clear mechanism of RGS19 in lung cancer was reported [29]. Besides, physiological functions of most RGS proteins in immune response are largely unknown [30]. Our study first demonstrated RGS19 could be a risk factor for poor prognosis, and also correlated with the expression of several immune checkpoint and the infiltration of Tregs and Macrophages (Supplementary Fig. 2, Fig. 7A). This discovery provides a new perspective that RGS19 may participate in immune process regulation, which worth further studies. PINK1 (PTEN induced kinase 1) mediates the recruitment of Parkin to mitochondria, which facilitates the elimination of the injured mitochondria by autophagy. It also has been proved to play crucial roles in the genesis and development of tumor [31]. In lung carcinoma tissue, the expression of PINK1 was raised, which was associated with a poor prognosis [32]. In recent years, PINK1 was also found as a repressor of the immune system and played a key role in adaptive immunity by repressing presentation of mitochondrial antigens [33]. Similar with previous studies, our study reported PINK1 was a risk factor for worse outcome. Moreover, PINK1 was found to be associated with the expression of PD-1 and CTLA4 as well as the infiltration of Tregs and macrophages. CTSD (Cathepsin D) is a key protein for lysosomal function that is necessary for autophagy in cancer cells [34]. Although CTSD is expressed at high levels in many cells of the immune system, but its role in immune function is still not well understood. In the present investigation, we observed that, similar with the other three genes, CTSD was correlated with poor survival and immunosuppressive status as well.

Taken together, it is reasonable to believe that the combination of these four genes has robust prediction value in LUSC, and the four-gene signature could stratify patients with different immune contexture, which is critical in the context of current immunotherapy. Moreover, GSEA analysis was employed to make the functional annotation, and we found the more abundant negative-regulation of immune responses and processes in the high autophagy-related score group. Later, survival analyses were employed to examine whether the infiltration of 28 infiltrating immune cell subtypes were prognostic and it turned out that only macrophage and Treg cells have a significantly negative correlation with overall survival. While, these two types of cells delivering pro-tumor suppression were consistently enriched in high-risk group. Recent studies have shown that autophagy significantly controls immune responses by modulating the functions of immune cells and the relationship between autophagy and immunity are complicated [35]. On one hand, autophagy has been shown to be important for priming of tumor-specific CD8 + T cells, and inhibition of autophagy would impair systemic immunity [36]. However, on the other

hand, the induction of autophagy may also benefit tumor cells escape from immune surveillance [35]. A recent report indicated that immunosuppressive Treg cells are critically dependent on autophagy [37]. Results showed that autophagy is active in Treg cells and supports their lineage stability and survival fitness [37]. While, for macrophage, autophagy regulates cellular development of monocytes, resulting in the disturbance of macrophage differentiation. Thus, our findings that high-risk group with higher expression of the four autophagy-related genes had an increased infiltration level of Treg cells and macrophages should be noticed. Moreover, based on estimate/immune/stromal scores from the ESTIMATE algorithm, we found that both the estimate score and immune score of high-risk group are higher and patients with higher scores tended to have a worse outcome.

The high-risk group presented a comparatively suppressed immune status, the phenotype of adaptive immune evasion. Actually, the infiltration of almost all immune cells were upregulated in high-risk group, including both the immune-suppressive subtypes and immune-stimulatory subtypes. This observation possibly suggested the presence of a feedback mechanism such that the recruitment or differentiation of cells specialized for immune suppression may be facilitated by anti-tumor inflammation. This could also be explained by our results that the immunosuppressive molecules points such as PD-1, CTLA4 was also higher in high-risk group, which means the presence of a suppressed pre-existing antitumor immunity that could be re-invigorated by anti PD-1/PD-L1 immunotherapy [38]. Besides, a previous review has been proposed that four different types of tumor microenvironment exist based on the presence or absence of tumor-infiltrating lymphocytes (TILs) and PD-L1 expression [39]. Type I cancers (with higher PD-L1 + and TILs) are more likely to benefit to anti-PD-1/L1 therapy [39]. Thus, we speculated that the high-risk group are more likely to respond to ICIs.

Conclusion

In conclusion, this study developed a new autophagy-related four- gene prognostic risk signature, which could be applied as an independent prognostic indicator for LUSC patients. And the autophagy-related scores are bound up with immune phenotype of LUSC, with higher score indicating an immune-suppression status. This study provides a novel and comprehensive sight to the correlation of autophagy and immune landscape in the tumor microenvironment of LUSC.

Abbreviations

LUSC
Lung squamous cell carcinoma; NSCLC:Non-small cell lung cancer; ARG:Autophagy-related gene; TCGA:The Cancer Genome Atlas; GEO:Gene Expression Omnibus; ROC:Receiver operating characteristic; GSEA:Gene set enrichment analysis; ICIs:Immune checkpoint inhibitors; PD-1:Programmed cell death protein-1; PD-L1:Programmed death ligand-1; OS:Overall survival; DEGs:Differentially expressed genes; KEGG:Kyoto Encyclopedia of Genes and Genomes; AUC:Area under the curve; ssGSEA:Single-Sample Gene Set Enrichment Analysis; ESTIMATE:Estimation of Stromal and Immune cells in Malignant Tumor

Declarations

Ethics approval and consent to participate

Not applicable.

Consent for publication

Not applicable.

Availability of data and materials

Publicly available datasets were analyzed in this study. These can be found here: TCGA database (https://portal.gdc.cancer.gov/) and the NCBI Gene Expression Omnibus (https://www.ncbi.nlm.nih.gov/geo/).

Competing interests

The authors declare that the research was conducted in the absence of any commercial or financial relationships that could be construed as a potential conflict of interest.

Funding

Not applicable.

Authors' contributions

LL and JD contributed to the design of the study. LL, LX and ML contributed to the data collection and analysis. LL contributed to the paper writing. JD, KZ and TQ contributed to the revising work and the manuscript review. All authors read and approved the final manuscript.

Acknowledgement

The authors would like to thank the HADb, TCGA and GEO databases for the availability of the data.

References

1. Siegel RL, Miller KD, Jemal A: Cancer statistics, 2018. CA Cancer J Clin 2018, 68(1):7-30.
2. Torre LA, Siegel RL, Jemal A: Lung Cancer Statistics. Adv Exp Med Biol 2016, 893:1-19.
3. Zhao Y, Liu J, Cai X, Pan Z, Liu J, Yin W, Chen H, Xie Z, Liang H, Wang W et al: Efficacy and safety of first line treatments for patients with advanced epidermal growth factor receptor mutated, non-small cell lung cancer: systematic review and network meta-analysis. BMJ 2019, 367:l5460.
4. Bianco A, Perrotta F, Barra G, Malapelle U, Rocco D, De Palma R: Prognostic Factors and Biomarkers of Responses to Immune Checkpoint Inhibitors in Lung Cancer. Int J Mol Sci 2019, 20(19).

5. Amaravadi RK, Kimmelman AC, Debnath J: Targeting Autophagy in Cancer: Recent Advances and Future Directions. Cancer Discov 2019, 9(9):1167-1181.
6. Qu X, Yu J, Bhagat G, Furuya N, Hibshoosh H, Troxel A, Rosen J, Eskelinen EL, Mizushima N, Ohsumi Y et al: Promotion of tumorigenesis by heterozygous disruption of the beclin 1 autophagy gene. J Clin Invest 2003, 112(12):1809-1820.
7. Cheong H: Integrating autophagy and metabolism in cancer. Arch Pharm Res 2015, 38(3):358-371.
8. Yang A, Herter-Sprie G, Zhang H, Lin EY, Biancur D, Wang X, Deng J, Hai J, Yang S, Wong KK et al: Autophagy Sustains Pancreatic Cancer Growth through Both Cell-Autonomous and Nonautonomous Mechanisms. Cancer Discov 2018, 8(3):276-287.
9. Guo JY, Teng X, Laddha SV, Ma S, Van Nostrand SC, Yang Y, Khor S, Chan CS, Rabinowitz JD, White E: Autophagy provides metabolic substrates to maintain energy charge and nucleotide pools in Ras-driven lung cancer cells. Genes Dev 2016, 30(15):1704-1717.
10. Shibutani ST, Saitoh T, Nowag H, Munz C, Yoshimori T: Autophagy and autophagy-related proteins in the immune system. Nat Immunol 2015, 16(10):1014-1024.
11. Deng Y, Zhu L, Cai H, Wang G, Liu B: Autophagic compound database: A resource connecting autophagy-modulating compounds, their potential targets and relevant diseases. Cell Prolif 2018, 51(3):e12403.
12. Breiman L: Random forests. Mach Learn 2001, 45(1):5-32.
13. Heagerty PJ, Lumley T, Pepe MS: Time-dependent ROC curves for censored survival data and a diagnostic marker. Biometrics 2000, 56(2):337-344.
14. Subramanian A, Tamayo P, Mootha VK, Mukherjee S, Ebert BL, Gillette MA, Paulovich A, Pomeroy SL, Golub TR, Lander ES et al: Gene set enrichment analysis: a knowledge-based approach for interpreting genome-wide expression profiles. Proc Natl Acad Sci U S A 2005, 102(43):15545-15550.
15. Charoentong P, Finotello F, Angelova M, Mayer C, Efremova M, Rieder D, Hackl H, Trajanoski Z: Pan-cancer Immunogenomic Analyses Reveal Genotype-Immunophenotype Relationships and Predictors of Response to Checkpoint Blockade. Cell Rep 2017, 18(1):248-262.
16. Jia Q, Wu W, Wang Y, Alexander PB, Sun C, Gong Z, Cheng JN, Sun H, Guan Y, Xia X et al: Local mutational diversity drives intratumoral immune heterogeneity in non-small cell lung cancer. Nat Commun 2018, 9(1):5361.
17. Yoshihara K, Shahmoradgoli M, Martinez E, Vegesna R, Kim H, Torres-Garcia W, Trevino V, Shen H, Laird PW, Levine DA et al: Inferring tumour purity and stromal and immune cell admixture from expression data. Nat Commun 2013, 4:2612.
18. Siriwardhana C, Khadka VS, Chen JJ, Deng Y: Development of a miRNA-seq based prognostic signature in lung adenocarcinoma. Bmc Cancer 2019, 19(1):34.
19. Lin T, Fu Y, Zhang X, Gu J, Ma X, Miao R, Xiang X, Niu W, Qu K, Liu C et al: A seven-long noncoding RNA signature predicts overall survival for patients with early stage non-small cell lung cancer. Aging (Albany NY) 2018, 10(9):2356-2366.

20. Li B, Cui Y, Diehn M, Li R: Development and Validation of an Individualized Immune Prognostic Signature in Early-Stage Nonsquamous Non-Small Cell Lung Cancer. JAMA Oncol 2017, 3(11):1529-1537.
21. Liu G, Pei F, Yang F, Li L, Amin AD, Liu S, Buchan JR, Cho WC: Role of Autophagy and Apoptosis in Non-Small-Cell Lung Cancer. Int J Mol Sci 2017, 18(2).
22. Liu Y, Wu L, Ao H, Zhao M, Leng X, Liu M, Ma J, Zhu J: Prognostic implications of autophagy-associated gene signatures in non-small cell lung cancer. Aging (Albany NY) 2019, 11(23):11440-11462.
23. Galon J, Bruni D: Approaches to treat immune hot, altered and cold tumours with combination immunotherapies. Nat Rev Drug Discov 2019, 18(3):197-218.
24. Safa AR: c-FLIP, a master anti-apoptotic regulator. Exp Oncol 2012, 34(3):176-184.
25. Safa AR, Pollok KE: Targeting the Anti-Apoptotic Protein c-FLIP for Cancer Therapy. Cancers (Basel) 2011, 3(2):1639-1671.
26. Micheau O: Cellular FLICE-inhibitory protein: an attractive therapeutic target? Expert Opin Ther Targets 2003, 7(4):559-573.
27. McLornan DP, Barrett HL, Cummins R, McDermott U, McDowell C, Conlon SJ, Coyle VM, Van Schaeybroeck S, Wilson R, Kay EW et al: Prognostic significance of TRAIL signaling molecules in stage II and III colorectal cancer. Clin Cancer Res 2010, 16(13):3442-3451.
28. Wang Y, Li JJ, Ba HJ, Wang KF, Wen XZ, Li DD, Zhu XF, Zhang XS: Down Regulation of c-FLIPL Enhance PD-1 Blockade Efficacy in B16 Melanoma. Front Oncol 2019, 9:857.
29. Tso PH, Yung LY, Wang Y, Wong YH: RGS19 stimulates cell proliferation by deregulating cell cycle control and enhancing Akt signaling. Cancer Lett 2011, 309(2):199-208.
30. Masuho I, Balaji S, Muntean BS, Skamangas NK, Chavali S, Tesmer JJG, Babu MM, Martemyanov KA: A Global Map of G Protein Signaling Regulation by RGS Proteins. Cell 2020, 183(2):503-521 e519.
31. O'Flanagan CH, Morais VA, Wurst W, De Strooper B, O'Neill C: The Parkinson's gene PINK1 regulates cell cycle progression and promotes cancer-associated phenotypes. Oncogene 2015, 34(11):1363-1374.
32. Zhang R, Gu J, Chen J, Ni J, Hung J, Wang Z, Zhang X, Feng J, Ji L: High expression of PINK1 promotes proliferation and chemoresistance of NSCLC. Oncol Rep 2017, 37(4):2137-2146.
33. Matheoud D, Cannon T, Voisin A, Penttinen AM, Ramet L, Fahmy AM, Ducrot C, Laplante A, Bourque MJ, Zhu L et al: Intestinal infection triggers Parkinson's disease-like symptoms in Pink1(-/-) mice. Nature 2019, 571(7766):565-569.
34. Hah YS, Noh HS, Ha JH, Ahn JS, Hahm JR, Cho HY, Kim DR: Cathepsin D inhibits oxidative stress-induced cell death via activation of autophagy in cancer cells. Cancer Lett 2012, 323(2):208-214.
35. Jiang GM, Tan Y, Wang H, Peng L, Chen HT, Meng XJ, Li LL, Liu Y, Li WF, Shan H: The relationship between autophagy and the immune system and its applications for tumor immunotherapy. Mol

Cancer 2019, 18.

36. Uhl M, Kepp O, Jusforgues-Saklani H, Vicencio JM, Kroemer G, Albert ML: Autophagy within the antigen donor cell facilitates efficient antigen cross-priming of virus-specific CD8(+) T cells. Cell Death Differ 2009, 16(7):991-1005.
37. Weil J, Long LY, Yang K, Guyl C, Shresthal S, Chen ZJ, Wu C, Voge P, Neale G, Green DR et al: Autophagy enforces functional integrity of regulatory T cells by coupling environmental cues and metabolic homeostasis. Nat Immunol 2016, 17(3):277-285.
38. Maleki Vareki S: High and low mutational burden tumors versus immunologically hot and cold tumors and response to immune checkpoint inhibitors. J Immunother Cancer 2018, 6(1):157.
39. Teng MW, Ngiow SF, Ribas A, Smyth MJ: Classifying Cancers Based on T-cell Infiltration and PD-L1. Cancer Res 2015, 75(11):2139-2145.

Tables

Table 1. Univariate Cox regression and multivariate Cox regression of risk score and clinical traits.

	Univariate Cox mode		Multivariate Cox mode	
Variables	HR (95% CI)	P Value	HR (95% CI)	P Value
gender	0.864 (0.556–1.344)	0.516	1.3669 (0.8617–2.168)	0.184
age	1.01 (0.988–1.032)	0.378	0.9946 (0.9715–1.018)	0.654
T stage	1.275 (0.999–1.629	0.051	1.0003 (0.7929–1.262)	0.998
N stage	1.331 (1.042–1.7)	0.022*	1.1868 (0.7597–1.854)	0.452
risk score	1.107 (1.093–1.122)	<0.0001****	1.1096 (1.0944–1.125)	<0.0001****

Figures

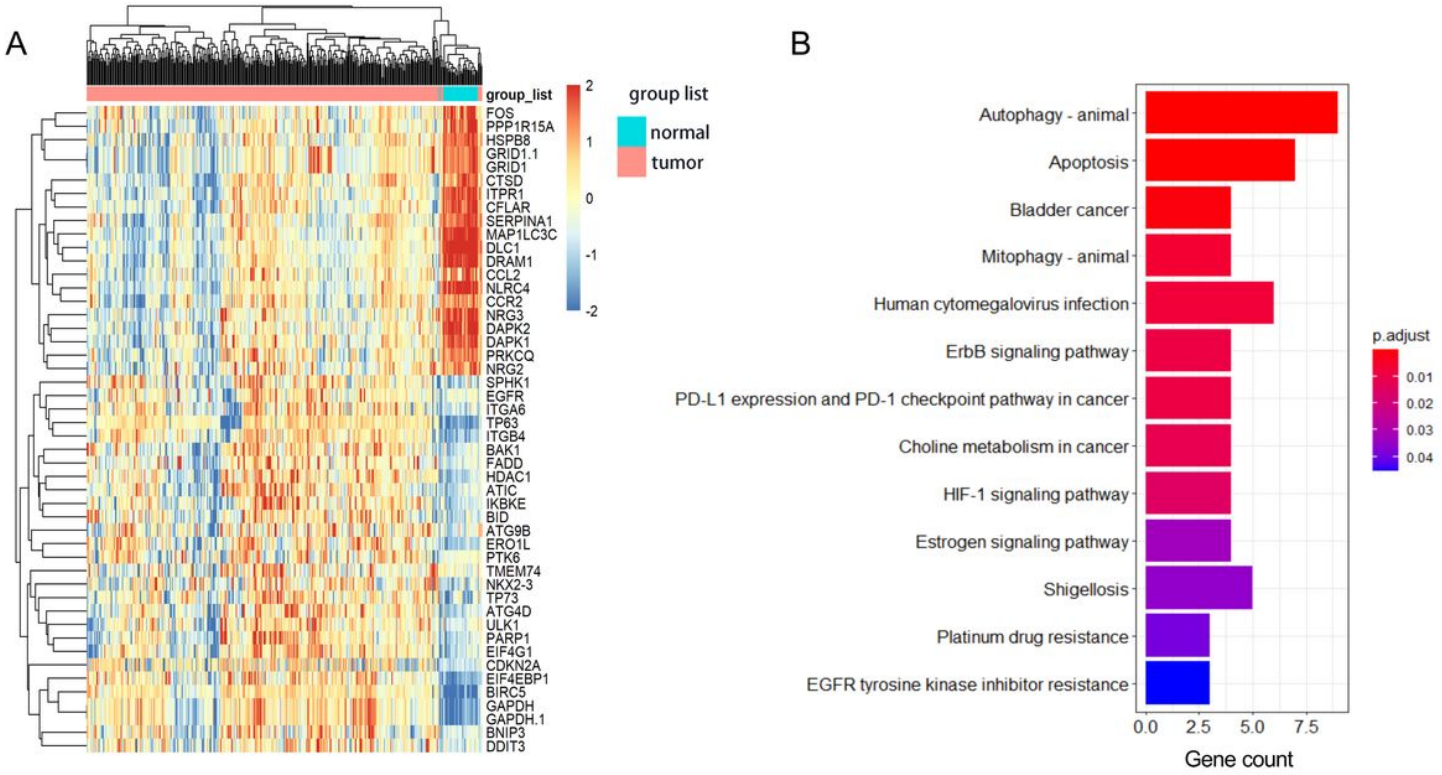

Figure 1

Results of differentially expressed analysis on ARGs and enrichment analysis of DE-ARGs. (A) A heatmap of 48 differentially expressed ARGs between 326 LUSC samples and 32 normal control. Each line represents a DE-ARG and each row means a sample. The expression levels of genes are displayed with colors in each cell (red for high and blue for low). (B) The enriched significant KEGG signal pathways of DE-ARGs. The color represents the statistical significance of the term. The length indicates the counts of enriched genes.

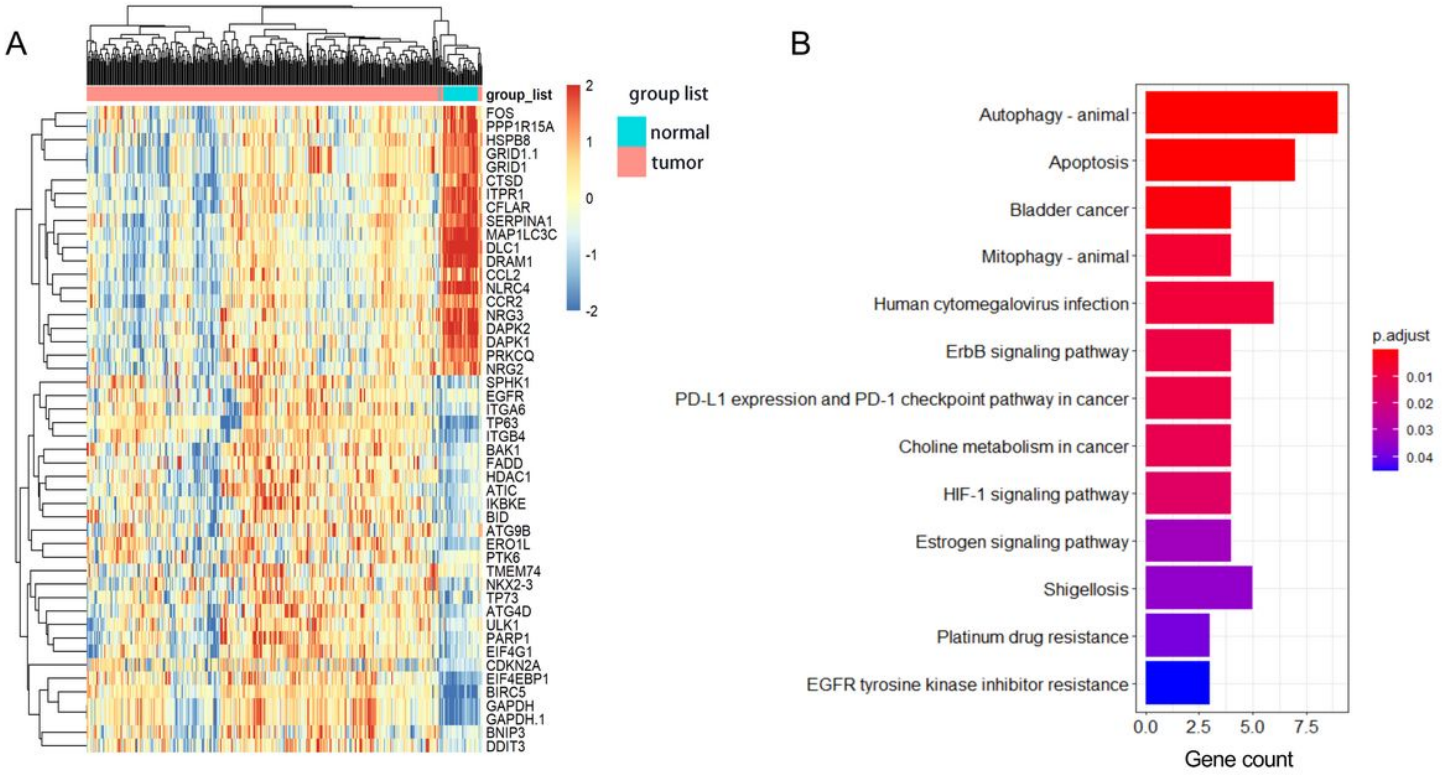

Figure 1

Results of differentially expressed analysis on ARGs and enrichment analysis of DE-ARGs. (A) A heatmap of 48 differentially expressed ARGs between 326 LUSC samples and 32 normal control. Each line represents a DE-ARG and each row means a sample. The expression levels of genes are displayed with colors in each cell (red for high and blue for low). (B) The enriched significant KEGG signal pathways of DE-ARGs. The color represents the statistical significance of the term. The length indicates the counts of enriched genes.

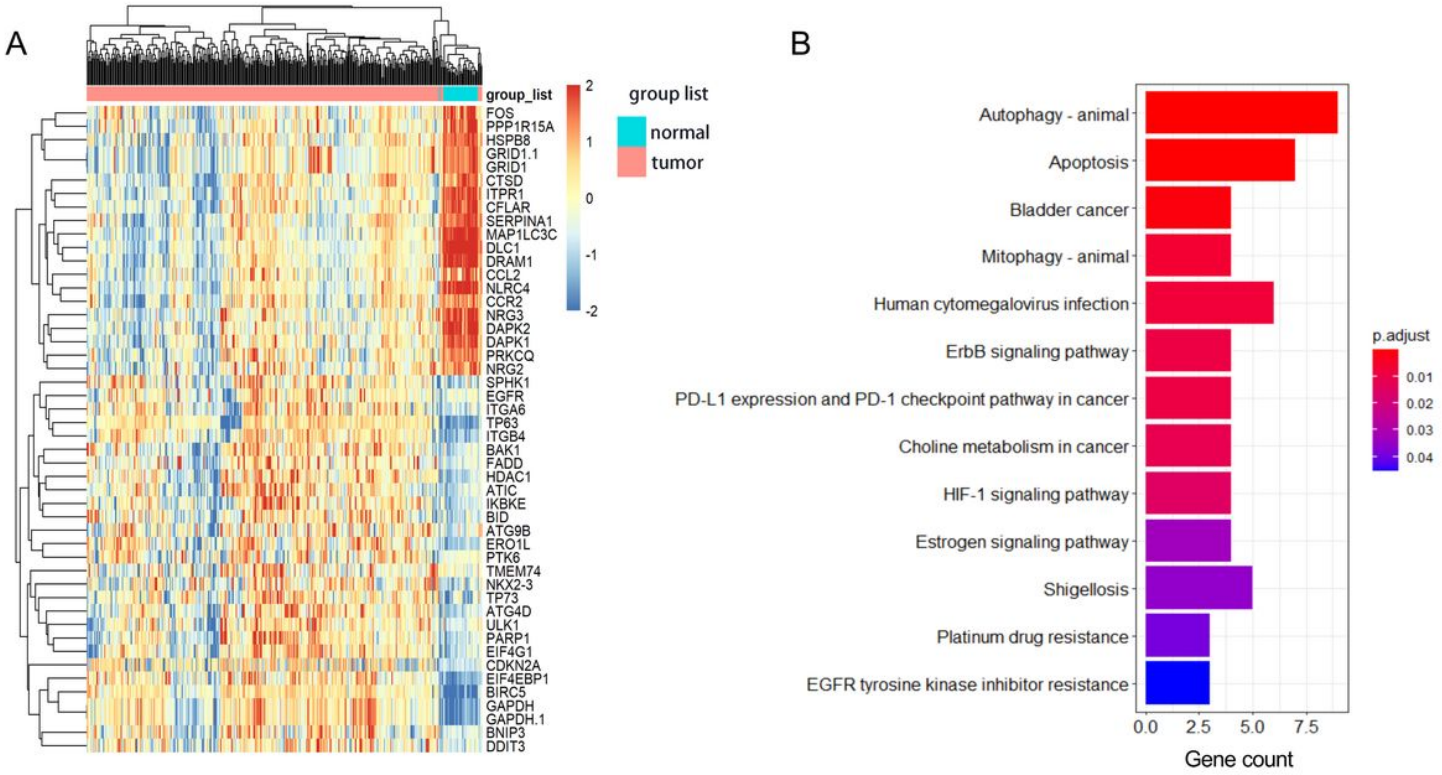

Figure 1

Results of differentially expressed analysis on ARGs and enrichment analysis of DE-ARGs. (A) A heatmap of 48 differentially expressed ARGs between 326 LUSC samples and 32 normal control. Each line represents a DE-ARG and each row means a sample. The expression levels of genes are displayed with colors in each cell (red for high and blue for low). (B) The enriched significant KEGG signal pathways of DE-ARGs. The color represents the statistical significance of the term. The length indicates the counts of enriched genes.

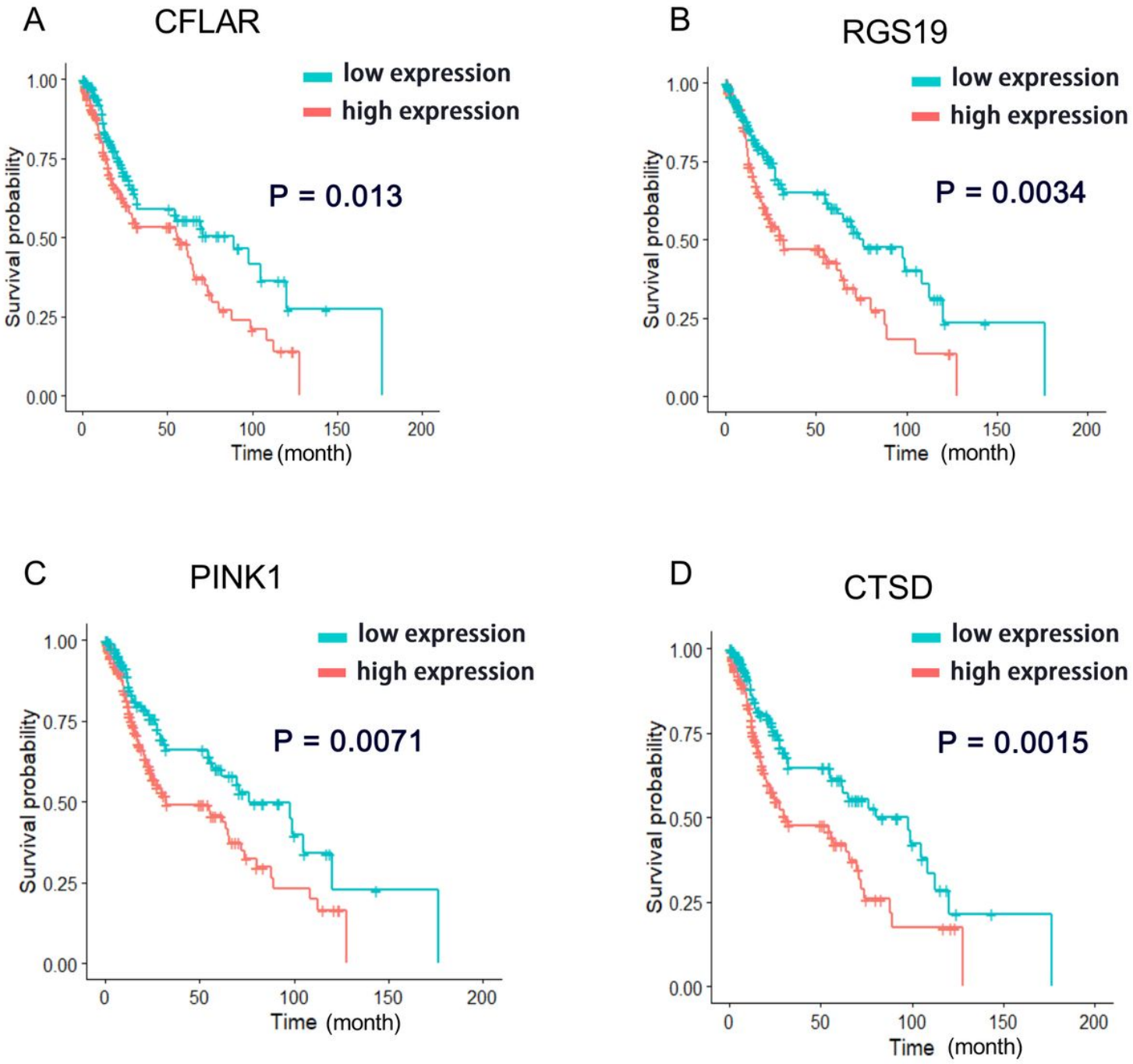

Figure 2

The results of survival analyses. Figure 2 A-D shows the Kaplan-Meier overall survival (OS) curves of CFLAR, RGS19, PINK1, CTSD for LUSC patients assigned to groups based on high and low expression levels of genes (cutoff=50%).

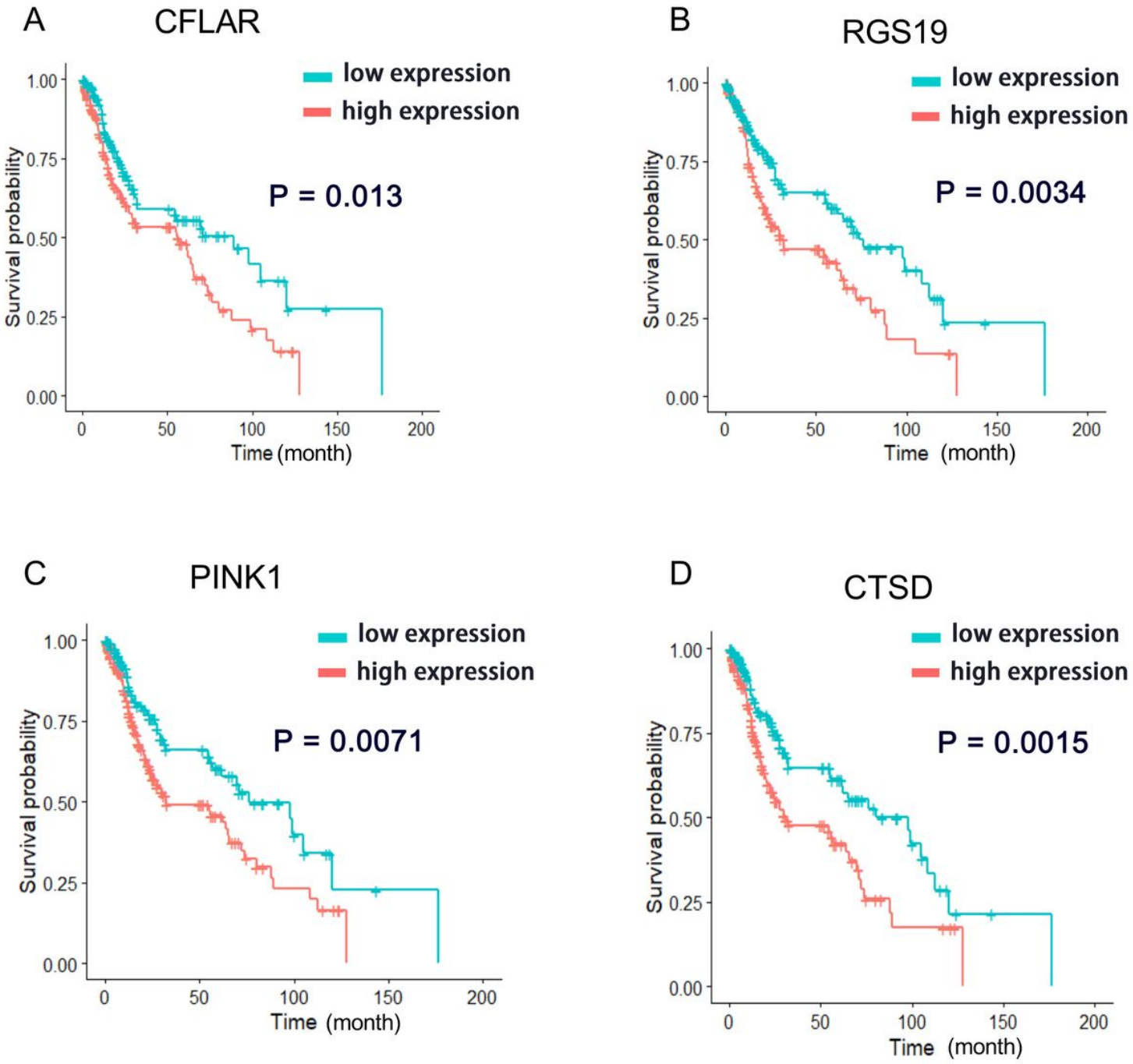

Figure 2

The results of survival analyses. Figure 2 A-D shows the Kaplan-Meier overall survival (OS) curves of CFLAR, RGS19, PINK1, CTSD for LUSC patients assigned to groups based on high and low expression levels of genes (cutoff=50%).

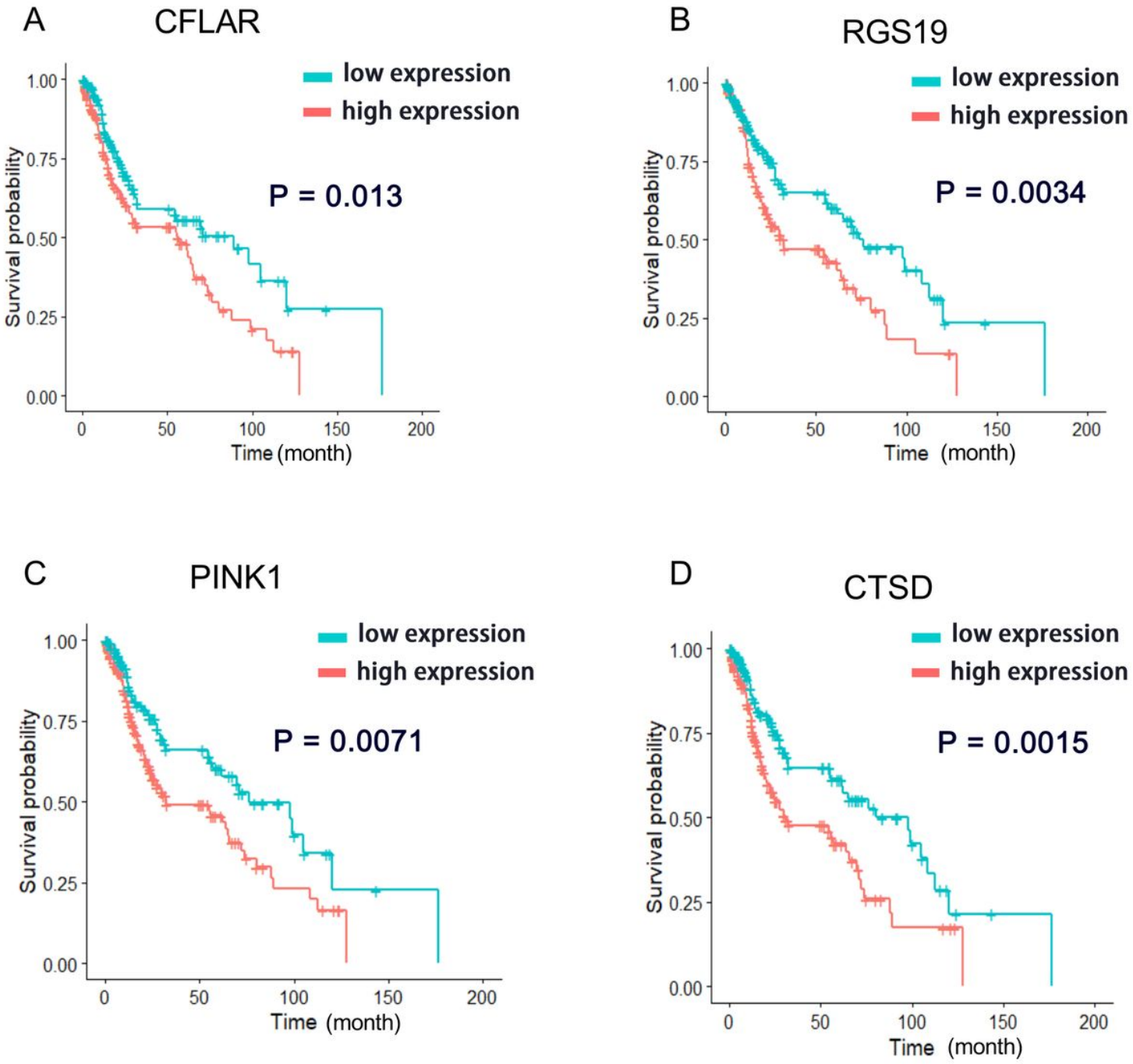

Figure 2

The results of survival analyses. Figure 2 A-D shows the Kaplan-Meier overall survival (OS) curves of CFLAR, RGS19, PINK1, CTSD for LUSC patients assigned to groups based on high and low expression levels of genes (cutoff=50%).

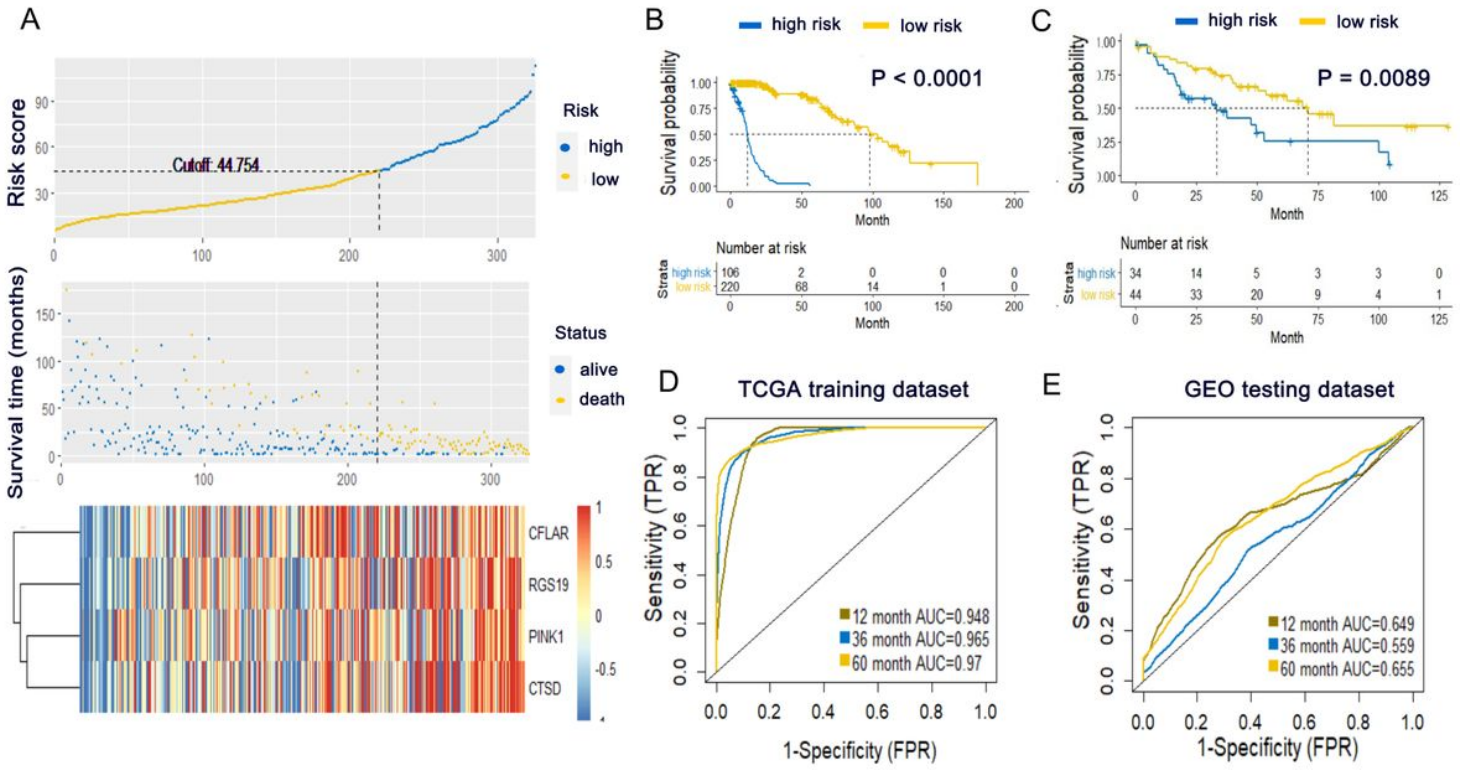

Figure 3

Construction and validation of the Autophagy-related prognostic signature. (A) Risk score distribution, survival status of each patient, and heatmaps of prognostic four-gene signature in TCGA cohorts. Patients were ranked by risk score. (B-C Kaplan-Meier survival curve of OS among LUSC patients from low-risk group and high-risk group in TCGA training dataset (B) and GEO testing dataset (C). (D-E) Receiver operating characteristic (ROC) curves of the risk score model in TCGA training dataset (D) and GEO testing dataset (E).

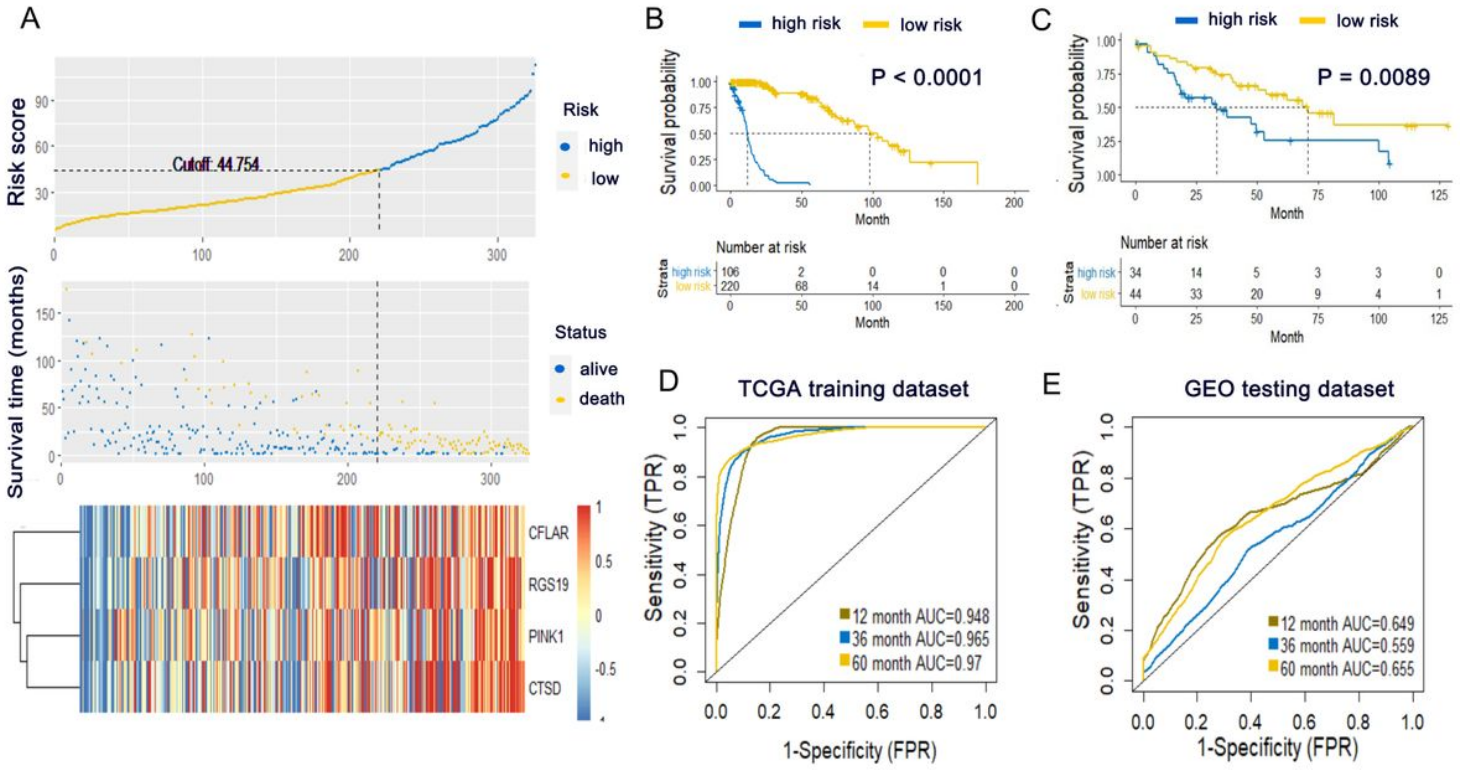

Figure 3

Construction and validation of the Autophagy-related prognostic signature. (A) Risk score distribution, survival status of each patient, and heatmaps of prognostic four-gene signature in TCGA cohorts. Patients were ranked by risk score. (B-C) Kaplan-Meier survival curve of OS among LUSC patients from low-risk group and high-risk group in TCGA training dataset (B) and GEO testing dataset (C). (D-E) Receiver operating characteristic (ROC) curves of the risk score model in TCGA training dataset (D) and GEO testing dataset (E).

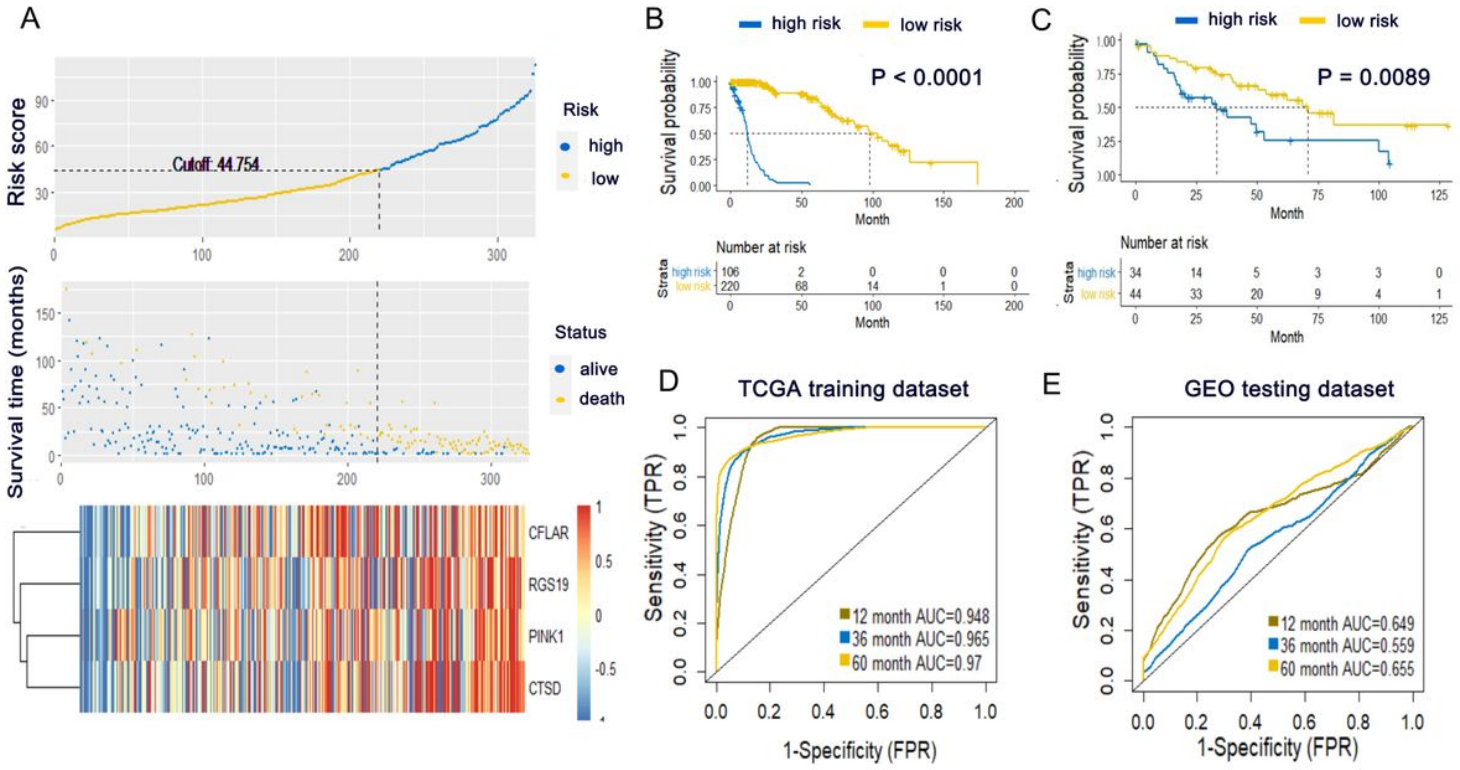

Figure 3

Construction and validation of the Autophagy-related prognostic signature. (A) Risk score distribution, survival status of each patient, and heatmaps of prognostic four-gene signature in TCGA cohorts. Patients were ranked by risk score. (B-C Kaplan-Meier survival curve of OS among LUSC patients from low-risk group and high-risk group in TCGA training dataset (B) and GEO testing dataset (C). (D-E) Receiver operating characteristic (ROC) curves of the risk score model in TCGA training dataset (D) and GEO testing dataset (E).

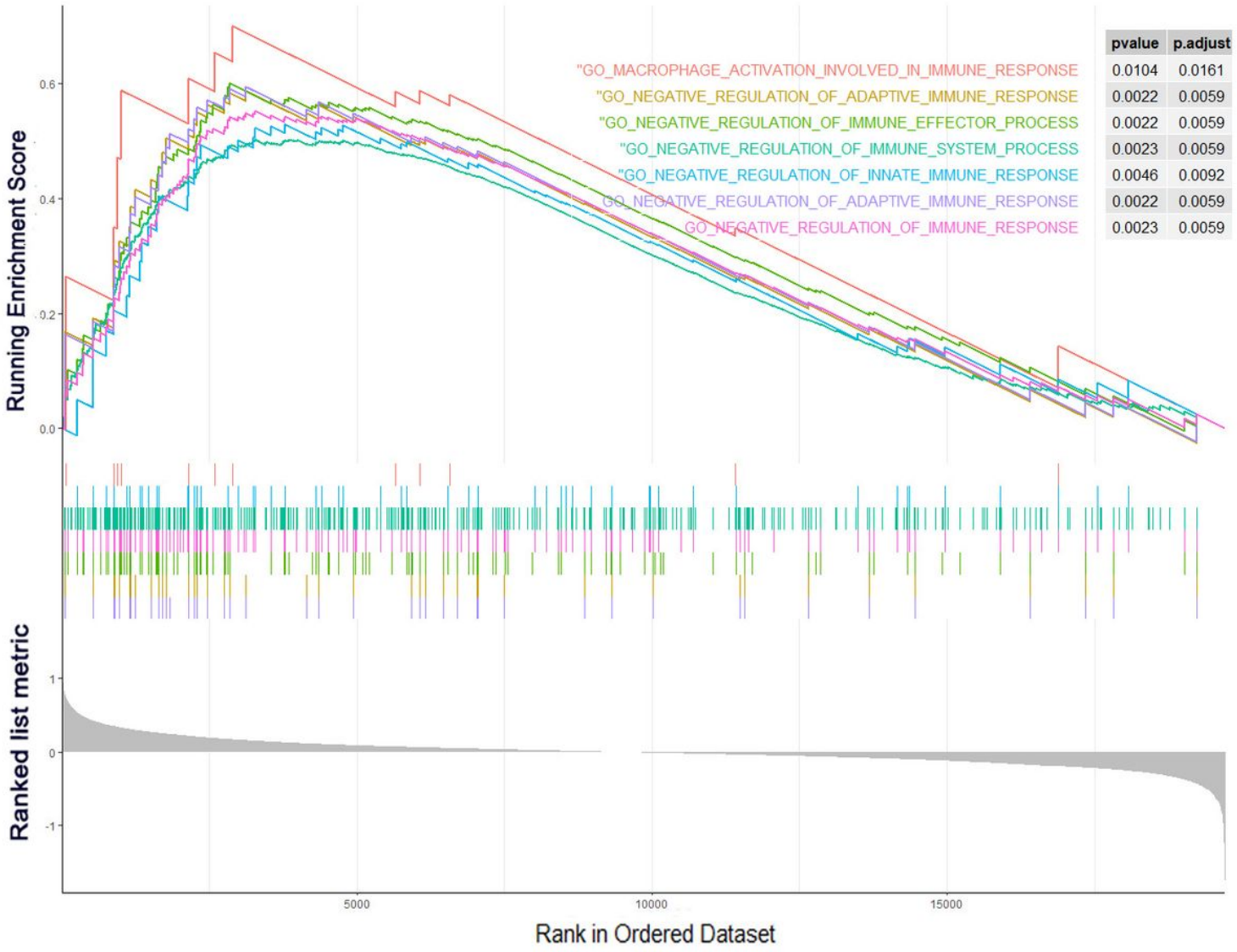

Figure 4

Pathways involved in negatively regulation of immune response by GSEA analyses. GSEA analyses displayed gene sets that were significantly enriched in high (up) or low (down) risk group. The pathways were colored, respectively. (Orange: Macrophage activation involved in immune response; Yellow: Negative regulation of adaptive immune response; Light green: Negative regulation of immune effector process; Aquamarine blue: Negative regulation of immune system process; Blue: Negative regulation of innate immune response; Violet: Negative regulation of adaptive immune response; Red violet: Negative response of immune response)

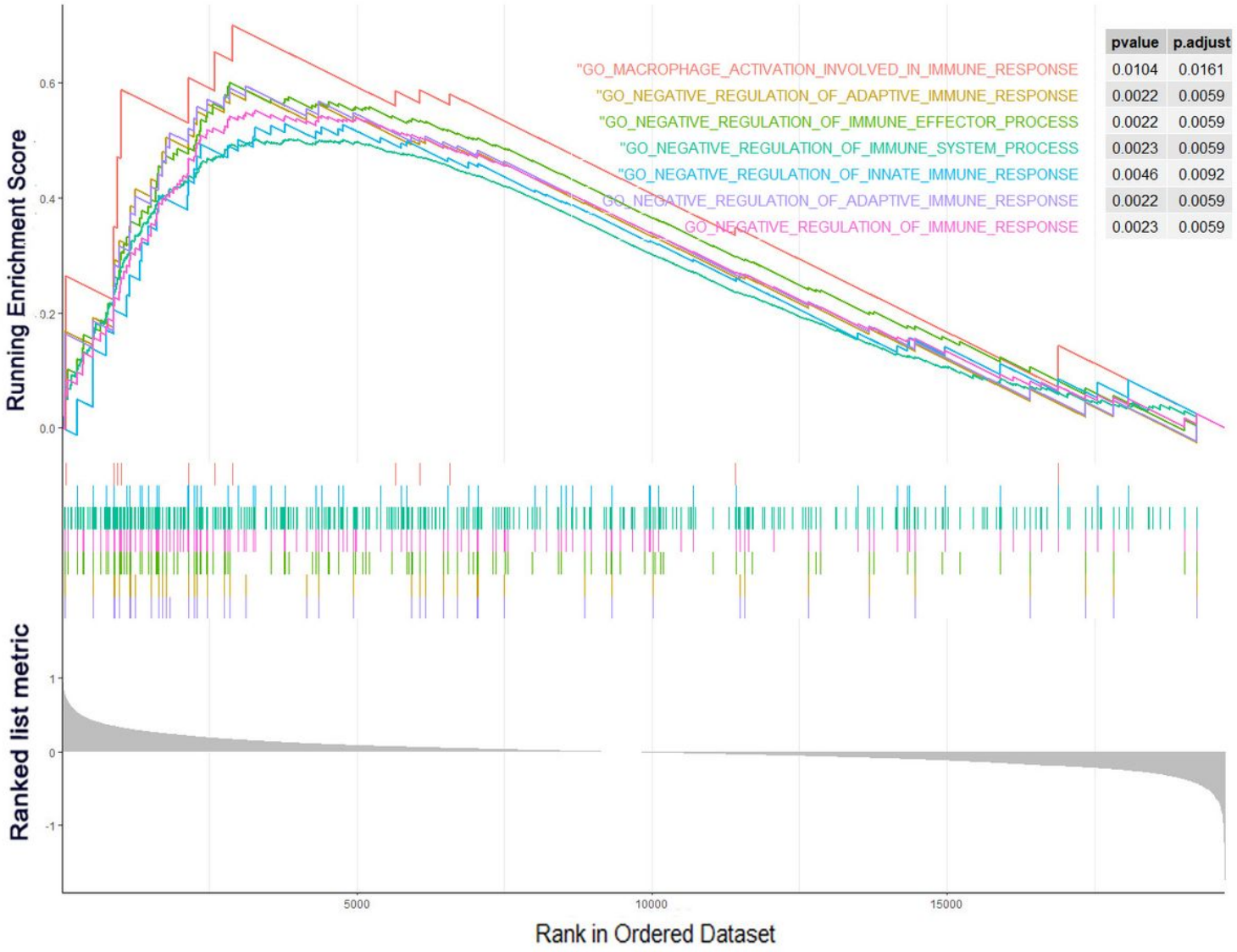

Figure 4

Pathways involved in negatively regulation of immune response by GSEA analyses. GSEA analyses displayed gene sets that were significantly enriched in high (up) or low (down) risk group. The pathways were colored, respectively. (Orange: Macrophage activation involved in immune response; Yellow: Negative regulation of adaptive immune response; Light green: Negative regulation of immune effector process; Aquamarine blue: Negative regulation of immune system process; Blue: Negative regulation of innate immune response; Violet: Negative regulation of adaptive immune response; Red violet: Negative response of immune response)

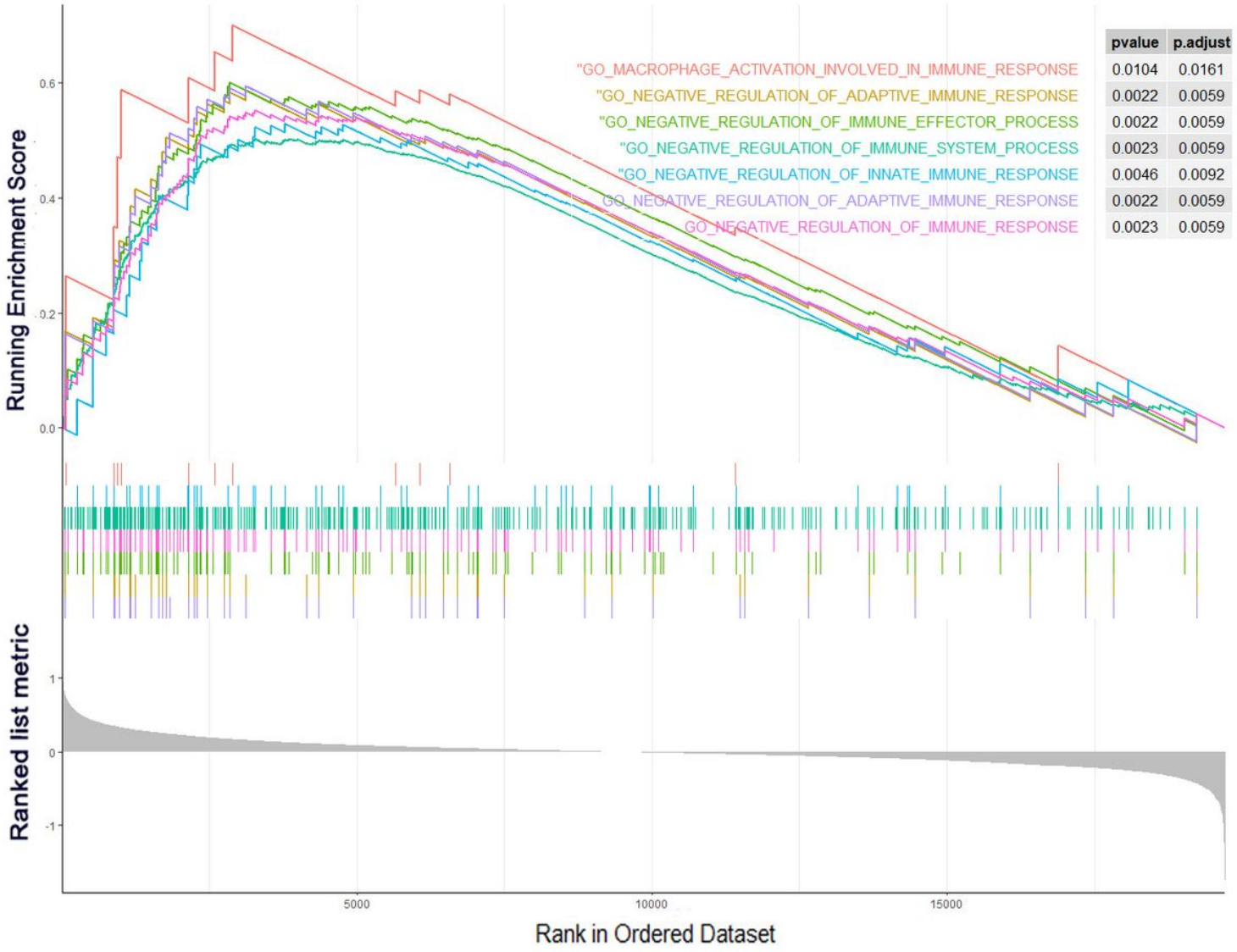

Figure 4

Pathways involved in negatively regulation of immune response by GSEA analyses. GSEA analyses displayed gene sets that were significantly enriched in high (up) or low (down) risk group. The pathways were colored, respectively. (Orange: Macrophage activation involved in immune response; Yellow: Negative regulation of adaptive immune response; Light green: Negative regulation of immune effector process; Aquamarine blue: Negative regulation of immune system process; Blue: Negative regulation of innate immune response; Violet: Negative regulation of adaptive immune response; Red violet: Negative response of immune response)

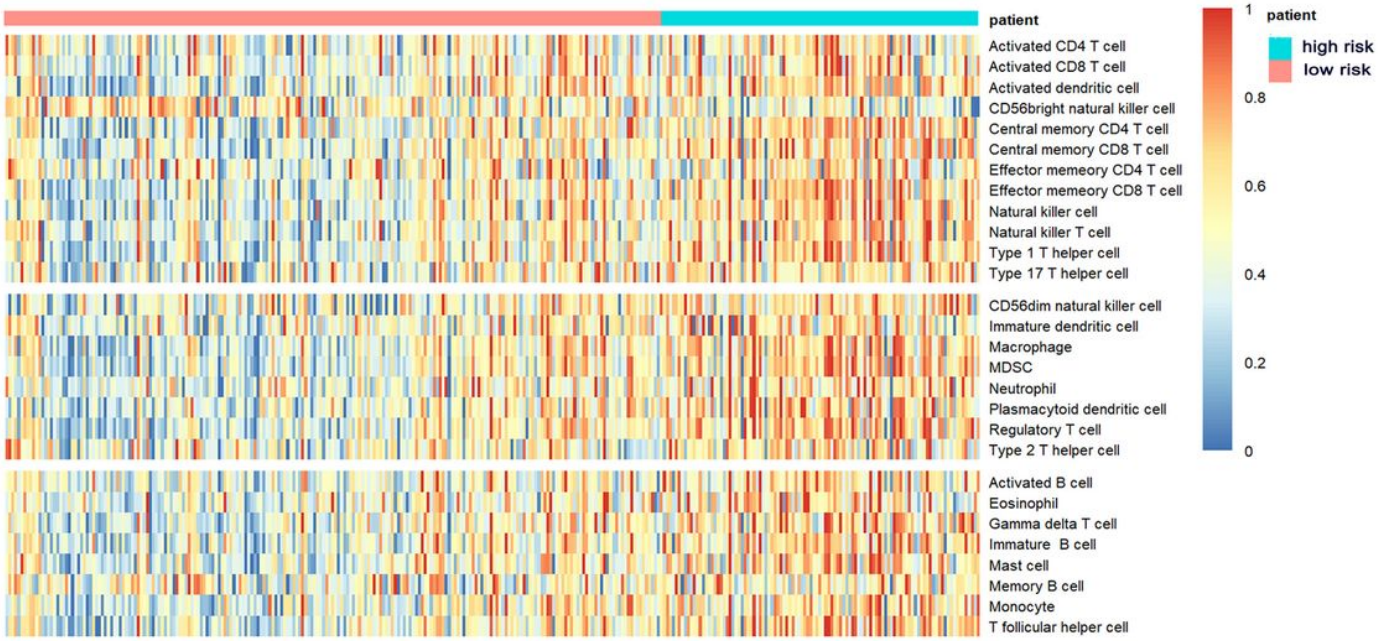

Figure 5

Heatmap of immune cell infiltration level of LUSC tumor samples in TCGA cohort. A Single-sample gene set enrichment analysis identifying the relative infiltration of 28 immune cell populations for LUSC tumor samples. Samples in the heatmap were ranked by risk score of each patient. The ssGSEA score which represents the relative infiltration of each cell type was normalized to unity distribution, for which zero is the minimal and one is the maximal score for each immune cell type. (red represents high and blue represents low infiltration). The three parts of the heatmap exhibited the three types of immune cells (anti-tumor immunity, pro-tumor immune-suppression, and other unclassified immune cells).

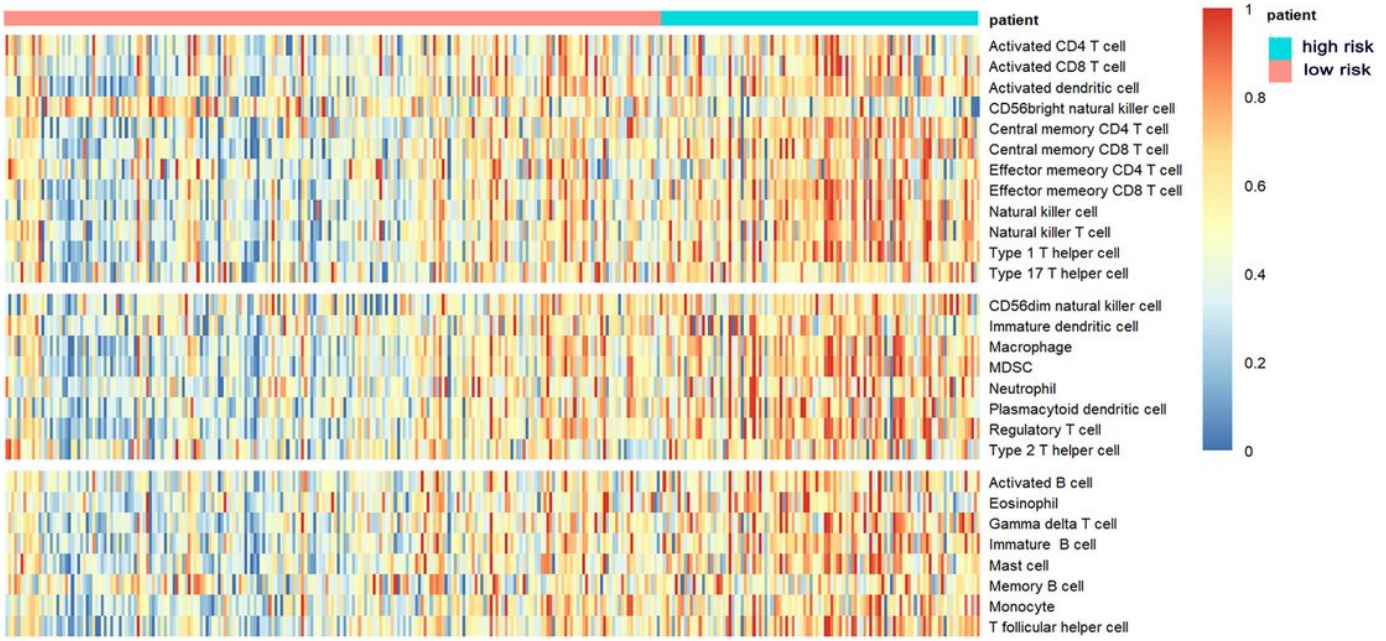

Figure 5

Heatmap of immune cell infiltration level of LUSC tumor samples in TCGA cohort. A Single-sample gene set enrichment analysis identifying the relative infiltration of 28 immune cell populations for LUSC tumor samples. Samples in the heatmap were ranked by risk score of each patient. The ssGSEA score which represents the relative infiltration of each cell type was normalized to unity distribution, for which zero is the minimal and one is the maximal score for each immune cell type. (red represents high and blue represents low infiltration). The three parts of the heatmap exhibited the three types of immune cells (anti-tumor immunity, pro-tumor immune-suppression, and other unclassified immune cells).

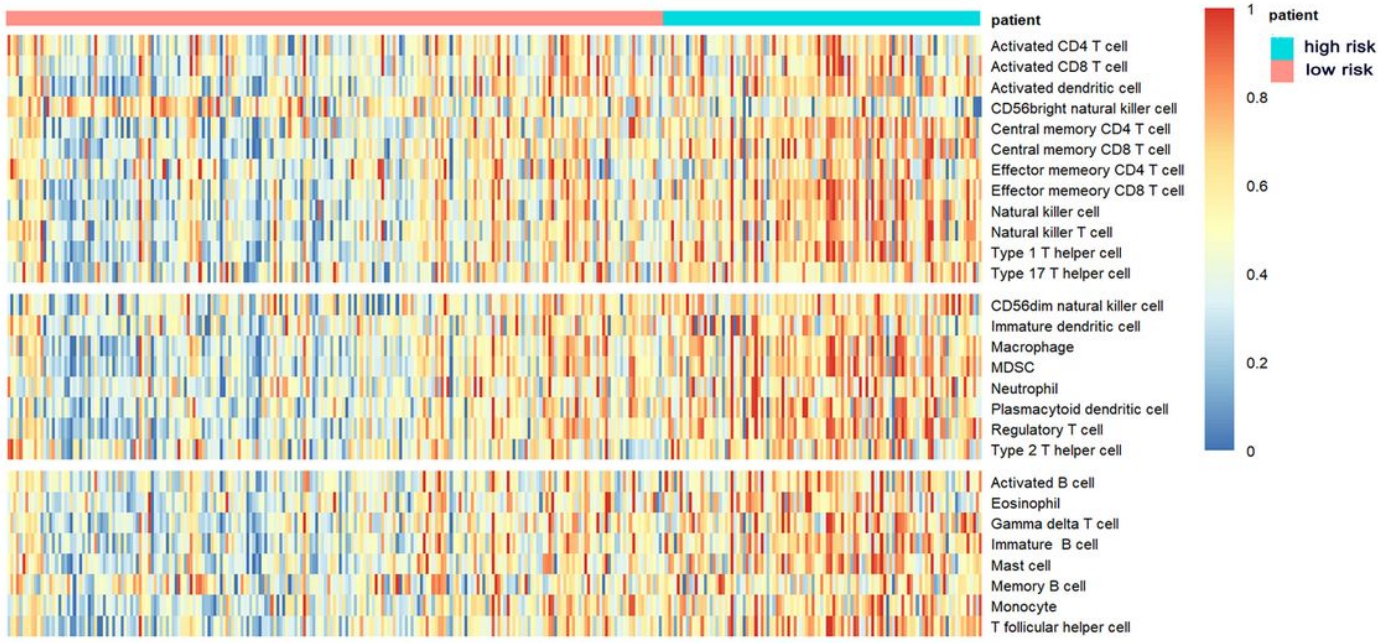

Figure 5

Heatmap of immune cell infiltration level of LUSC tumor samples in TCGA cohort. A Single-sample gene set enrichment analysis identifying the relative infiltration of 28 immune cell populations for LUSC tumor samples. Samples in the heatmap were ranked by risk score of each patient. The ssGSEA score which represents the relative infiltration of each cell type was normalized to unity distribution, for which zero is the minimal and one is the maximal score for each immune cell type. (red represents high and blue represents low infiltration). The three parts of the heatmap exhibited the three types of immune cells (anti-tumor immunity, pro-tumor immune-suppression, and other unclassified immune cells).

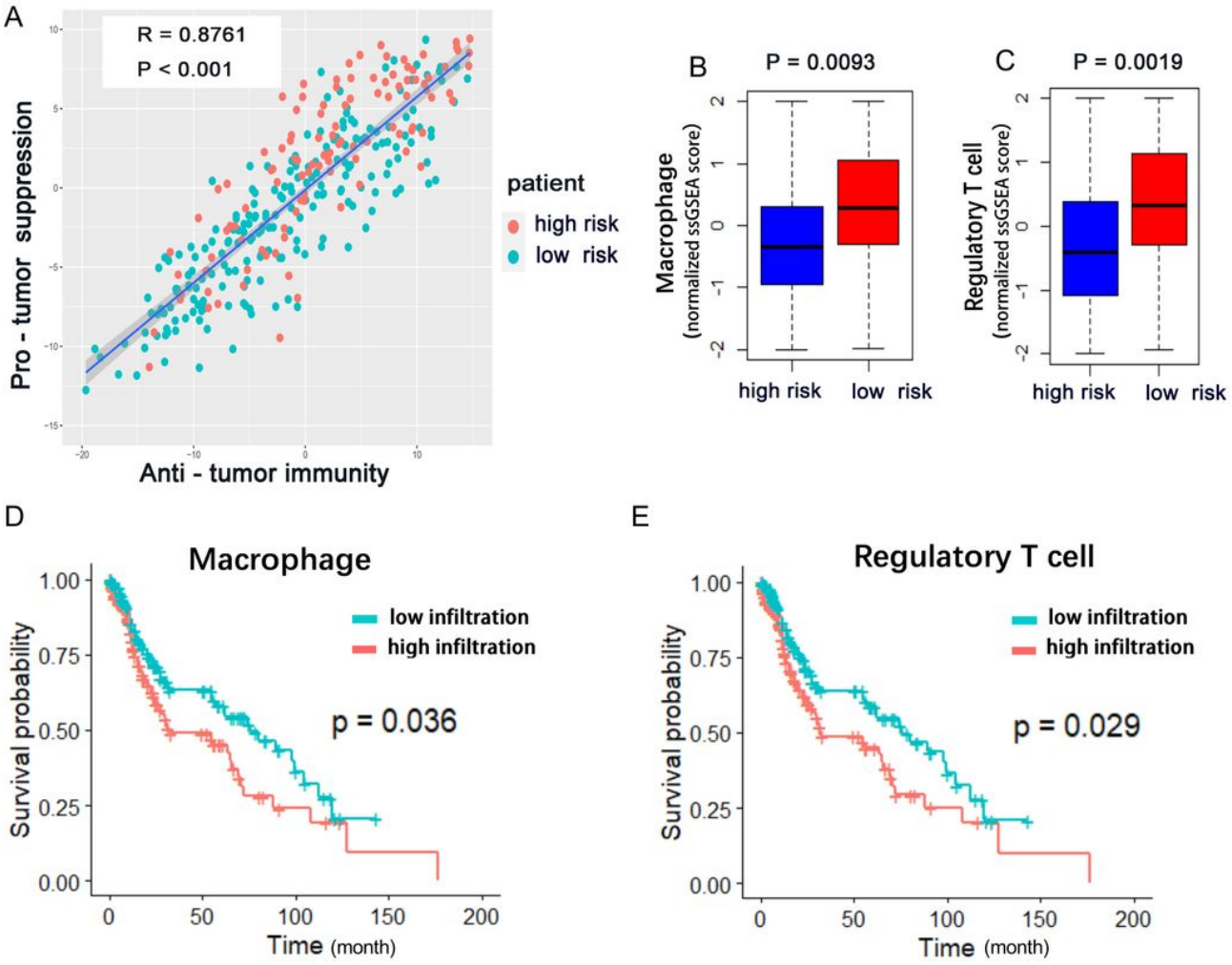

Figure 6

(A) Correlation between infiltration of cell types executing anti-tumor immunity and pro-tumor, immune suppressive functions. R coefficient of Pearson's correlation and P value were shown. (B) High risk group was associated with higher infiltration of Macrophage (Wilcox-test, P < 0.01).(C)High risk group was associated with higher infiltration of Regulatory T cell (Wilcox-test , P < 0.01). (D) Macrophage infiltration was negatively correlated with overall survival (Cutoff =50%, Log-Rank test, P < 0.05). (E) Regulatory T cell infiltration was negatively correlated with overall survival (Cutoff =50%, Log-Rank test, P < 0.05).

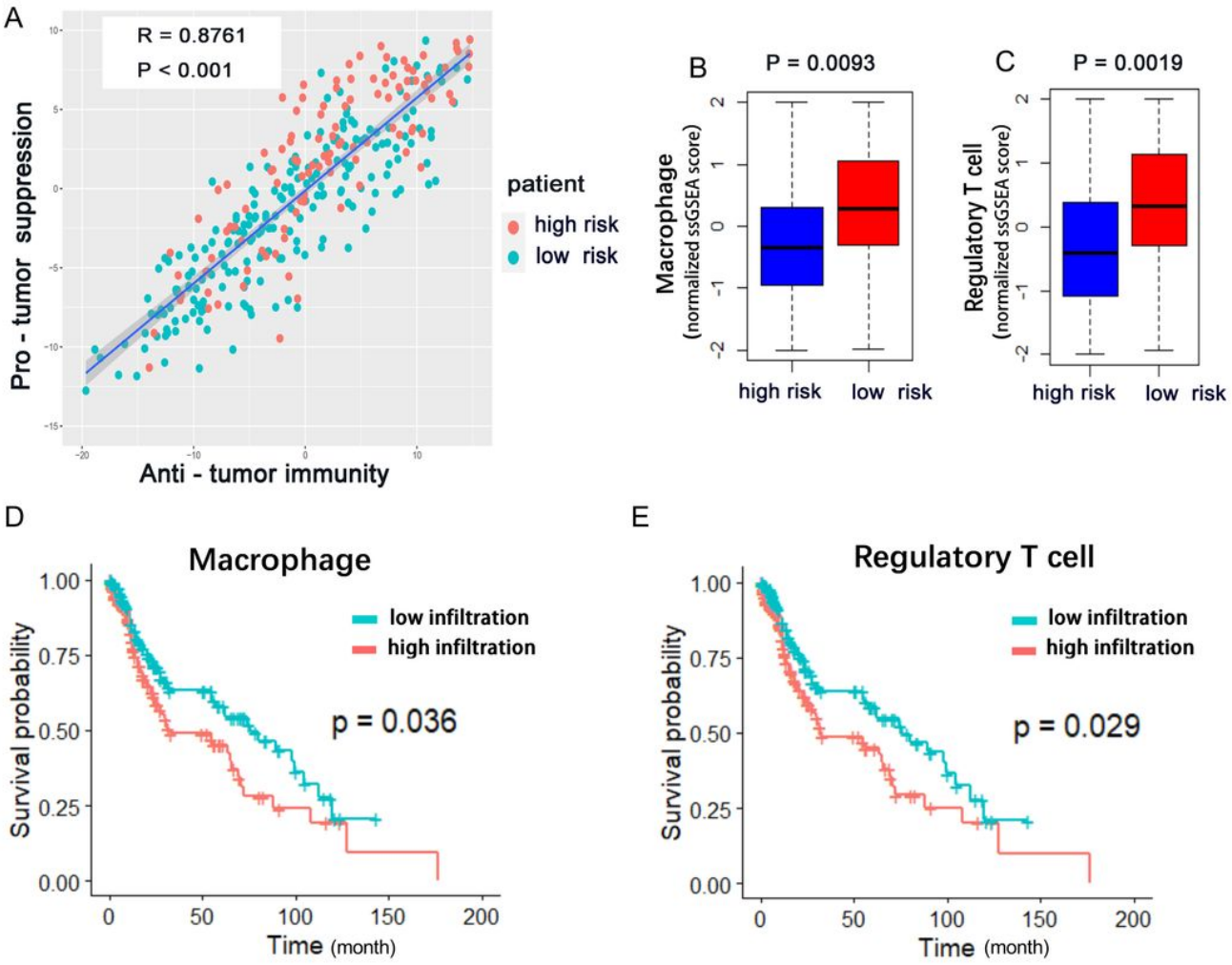

Figure 6

(A) Correlation between infiltration of cell types executing anti-tumor immunity and pro-tumor, immune suppressive functions. R coefficient of Pearson's correlation and P value were shown. (B) High risk group was associated with higher infiltration of Macrophage (Wilcox-test, P < 0.01).(C)High risk group was associated with higher infiltration of Regulatory T cell (Wilcox-test , P < 0.01). (D) Macrophage infiltration was negatively correlated with overall survival (Cutoff =50%, Log-Rank test, P < 0.05). (E) Regulatory T cell infiltration was negatively correlated with overall survival (Cutoff =50%, Log-Rank test, P < 0.05).

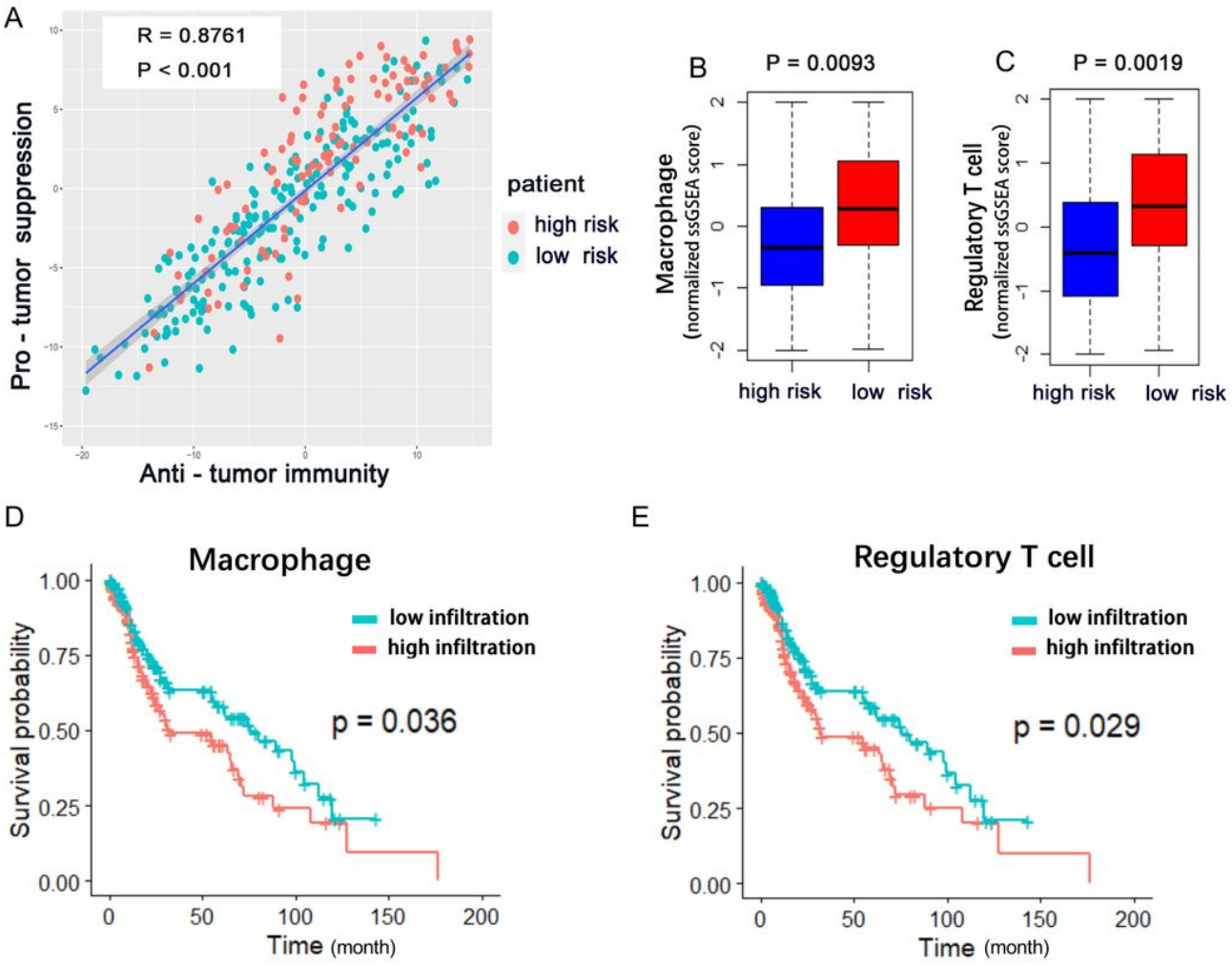

Figure 6

(A) Correlation between infiltration of cell types executing anti-tumor immunity and pro-tumor, immune suppressive functions. R coefficient of Pearson's correlation and P value were shown. (B) High risk group was associated with higher infiltration of Macrophage (Wilcox-test, P < 0.01).(C)High risk group was associated with higher infiltration of Regulatory T cell (Wilcox-test , P < 0.01). (D) Macrophage infiltration was negatively correlated with overall survival (Cutoff =50%, Log-Rank test, P < 0.05). (E) Regulatory T cell infiltration was negatively correlated with overall survival (Cutoff =50%, Log-Rank test, P < 0.05).

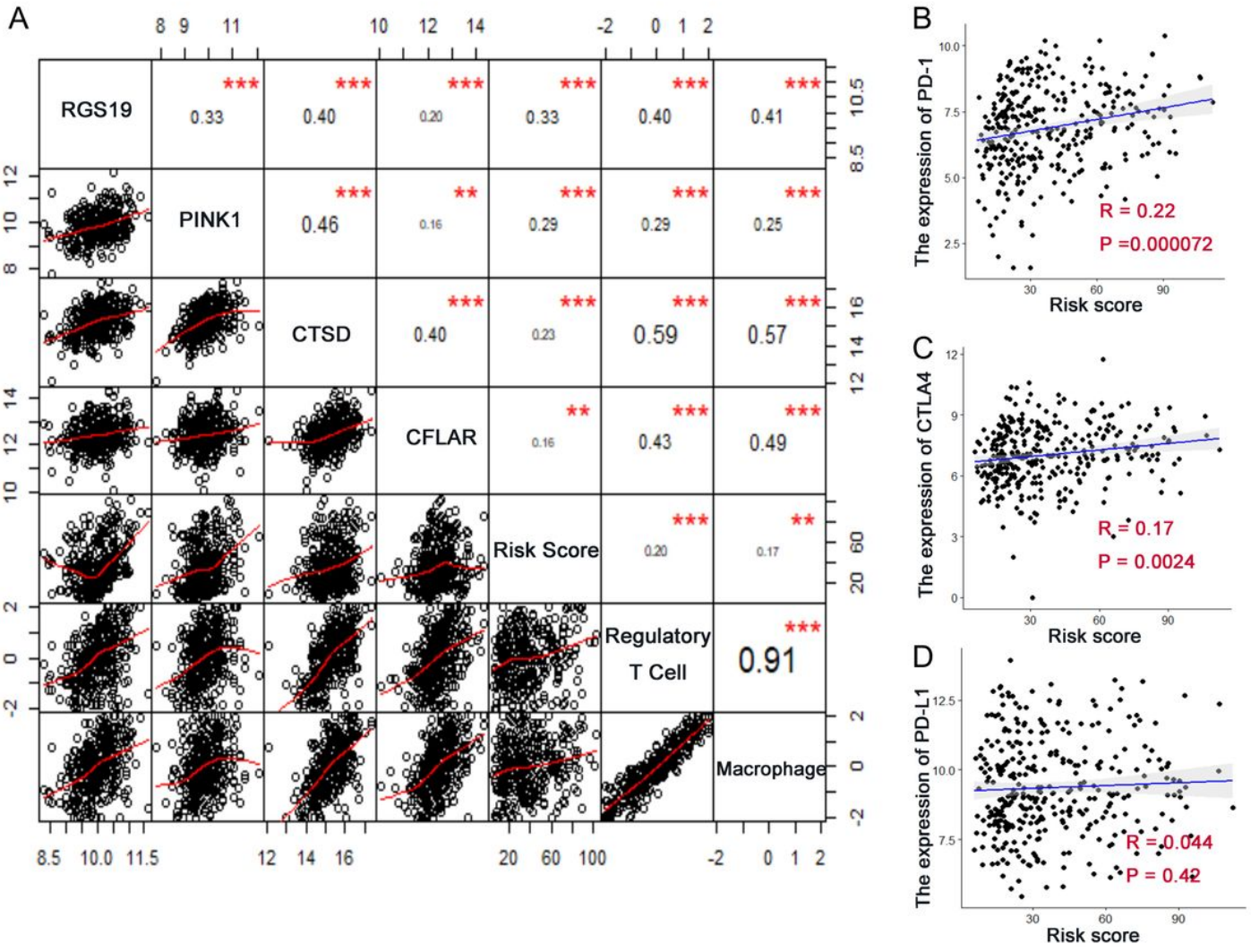

Figure 7

Correlations of risk score with genes expression, immunocyte infiltration and the immune checkpoint. (A) Correlation of the risk score with genes expression and immunocyte infiltration level. Pearson's correlation coefficient values with the significance level were shown on the top of the diagonal (** P < 0.01, *** P < 0.001). (B-D) Correlation of the risk score with the expression of several key immune checkpoints. (B) PD-1; (C) CTLA4; (D) PD-L1. Pearson's correlation coefficient values with the P value were shown

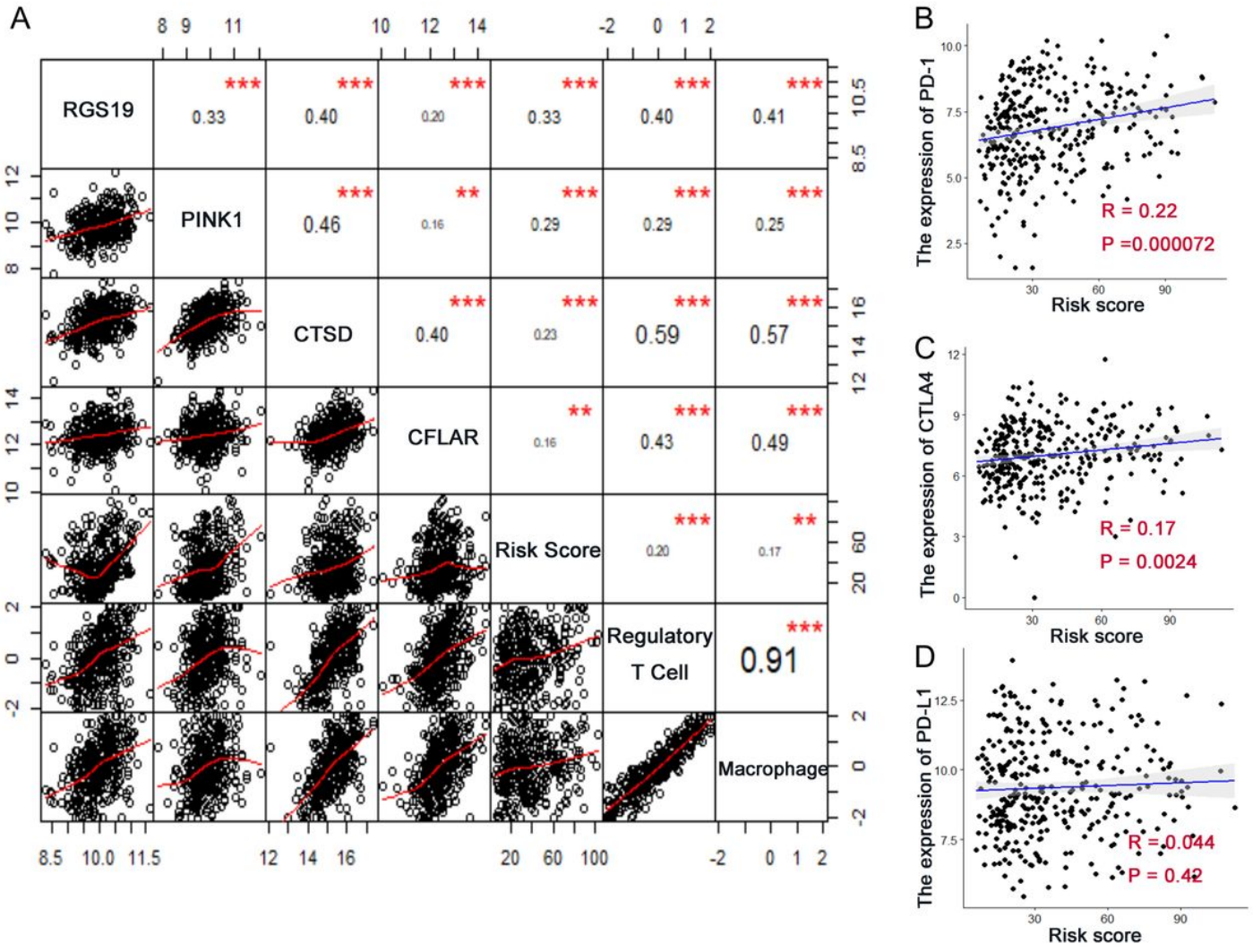

Figure 7

Correlations of risk score with genes expression, immunocyte infiltration and the immune checkpoint. (A) Correlation of the risk score with genes expression and immunocyte infiltration level. Pearson's correlation coefficient values with the significance level were shown on the top of the diagonal (** P < 0.01, *** P < 0.001). (B-D) Correlation of the risk score with the expression of several key immune checkpoints. (B) PD-1; (C) CTLA4; (D) PD-L1. Pearson's correlation coefficient values with the P value were shown

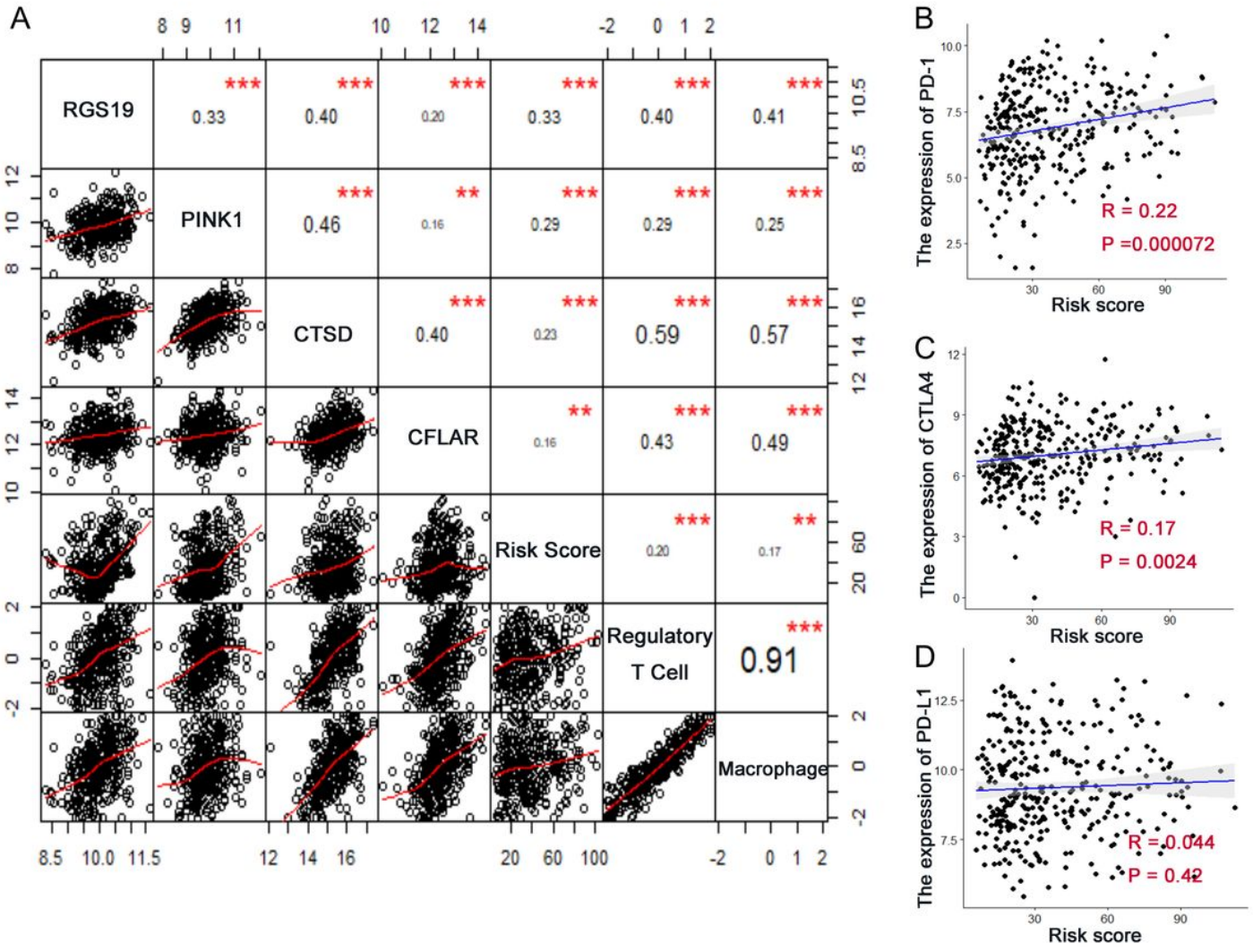

Figure 7

Correlations of risk score with genes expression, immunocyte infiltration and the immune checkpoint. (A) Correlation of the risk score with genes expression and immunocyte infiltration level. Pearson's correlation coefficient values with the significance level were shown on the top of the diagonal (** P < 0.01, *** P < 0.001). (B-D) Correlation of the risk score with the expression of several key immune checkpoints. (B) PD-1; (C) CTLA4; (D) PD-L1. Pearson's correlation coefficient values with the P value were shown

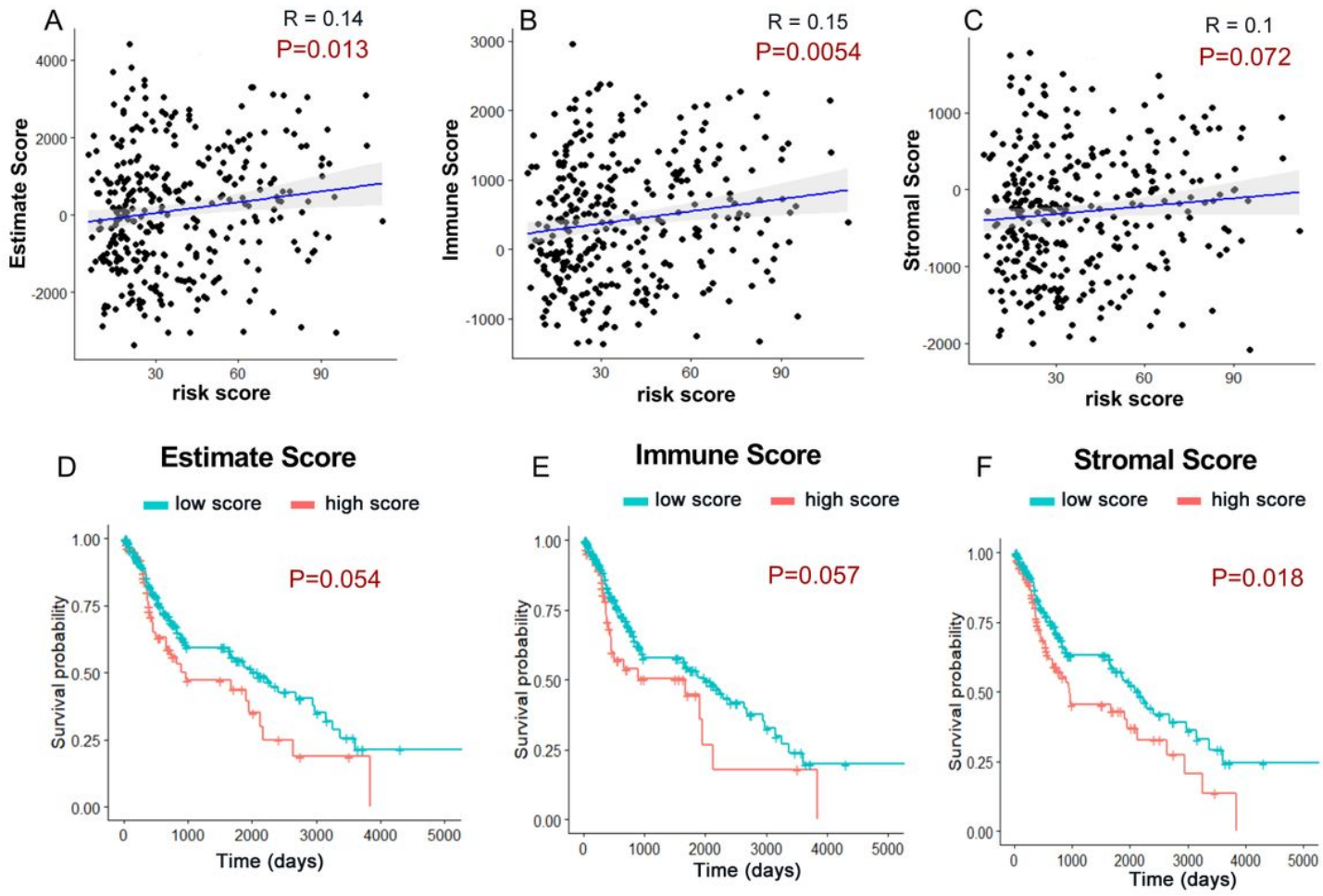

Figure 8

Correlation and survival analyses of estimate score, immune score and stromal score. (A-C) The correlations of risk score with estimate score, immune score and stromal score. Pearson's correlation coefficient values were showed. (D-F) The Kaplan-Meier overall survival curves for LUSC patients assigned to high and low score group (cutoff=50%). (D) Estimate score; (E) Immune score; (F) Stromal score.

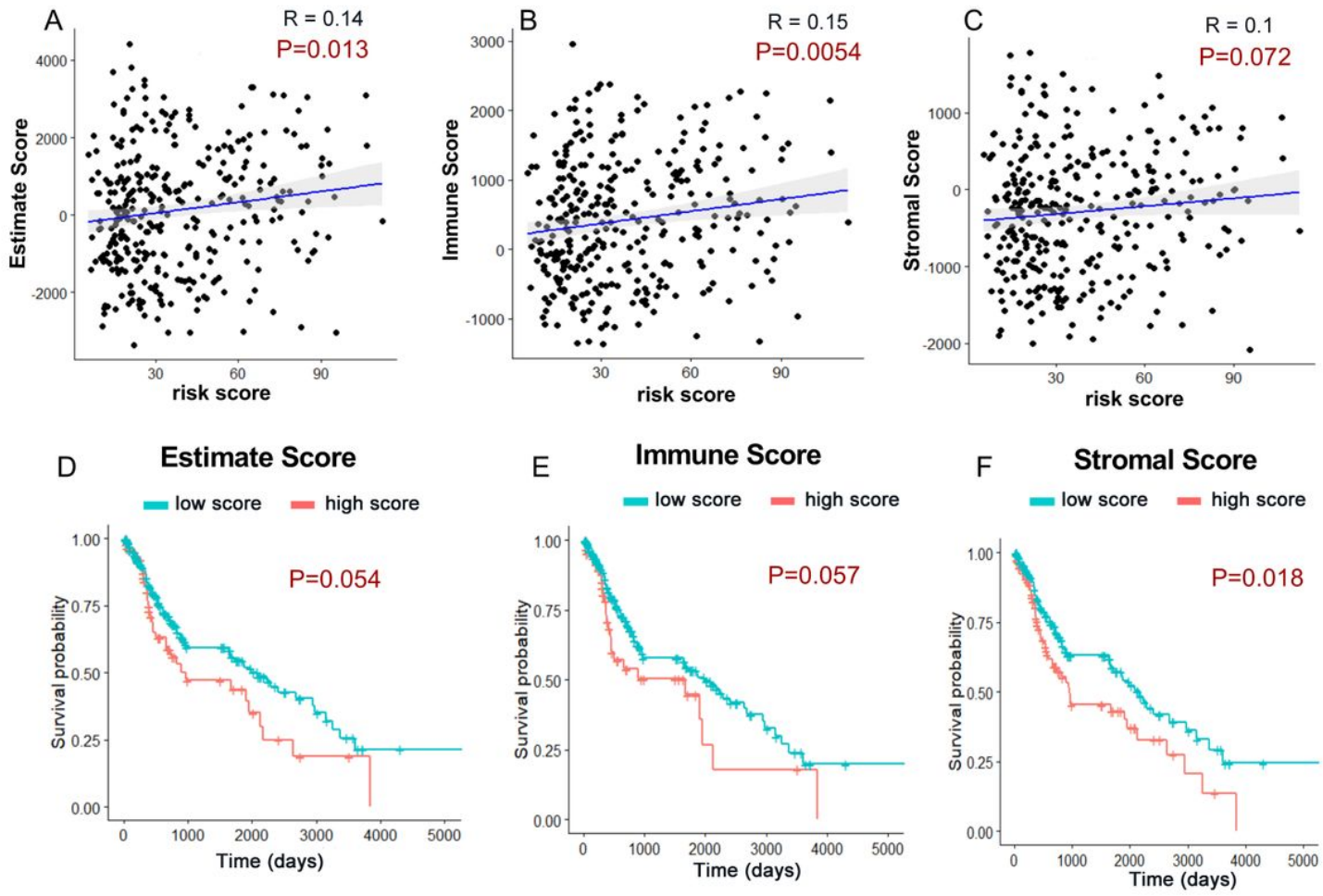

Figure 8

Correlation and survival analyses of estimate score, immune score and stromal score. (A-C) The correlations of risk score with estimate score, immune score and stromal score. Pearson's correlation coefficient values were showed. (D-F) The Kaplan-Meier overall survival curves for LUSC patients assigned to high and low score group (cutoff=50%). (D) Estimate score; (E) Immune score; (F) Stromal score.

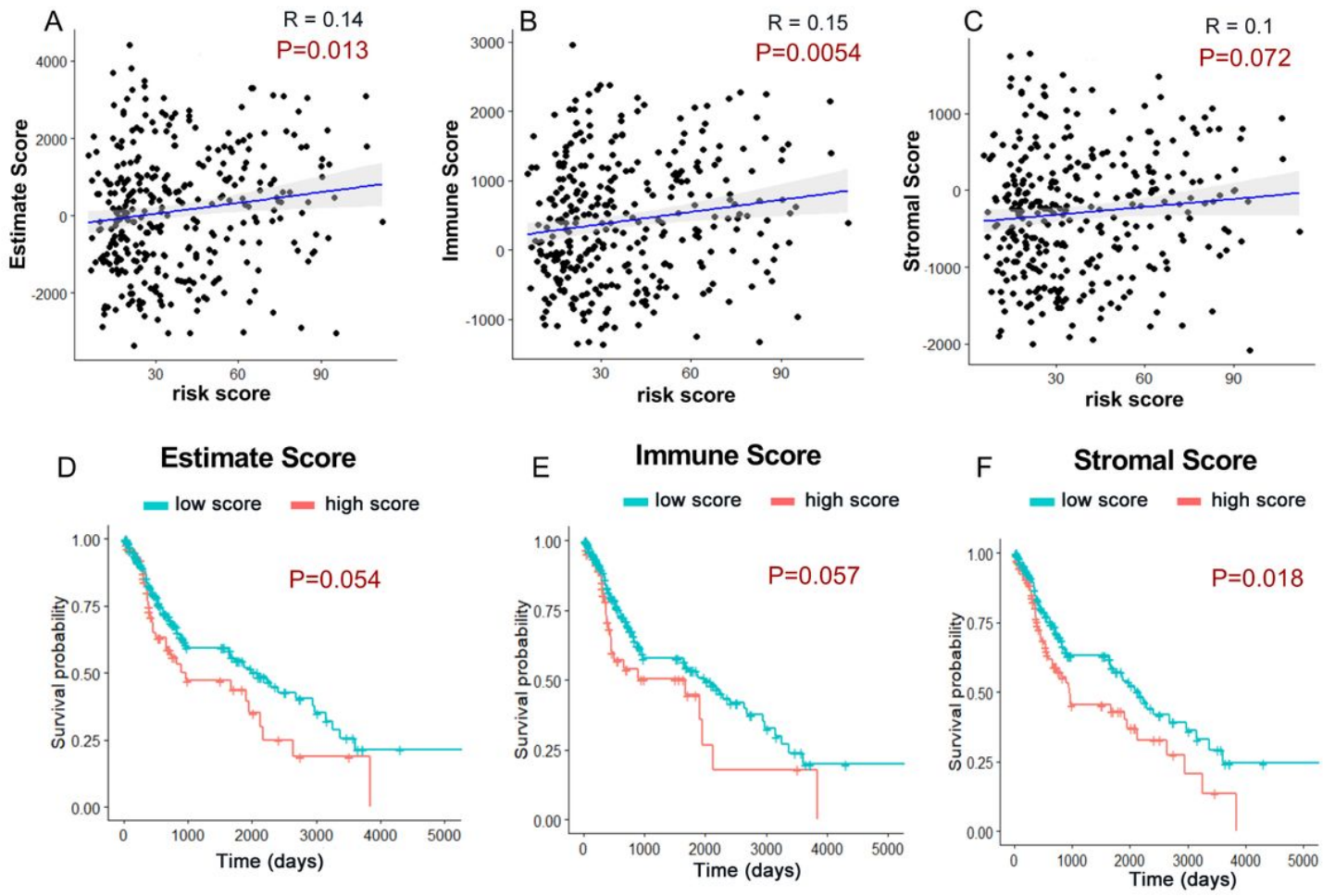

Figure 8

Correlation and survival analyses of estimate score, immune score and stromal score. (A-C) The correlations of risk score with estimate score, immune score and stromal score. Pearson's correlation coefficient values were showed. (D-F) The Kaplan-Meier overall survival curves for LUSC patients assigned to high and low score group (cutoff=50%). (D) Estimate score; (E) Immune score; (F) Stromal score.

Supplementary Files

This is a list of supplementary files associated with this preprint. Click to download.

- FigureS2.jpg
- FigureS2.jpg
- FigureS2.jpg
- FirureS1.jpg
- FirureS1.jpg
- FirureS1.jpg

- TableS1.xlsx
- TableS1.xlsx
- TableS1.xlsx
- TableS2.xlsx
- TableS2.xlsx
- TableS2.xlsx